MUCILAGE-RELATED10 Produces Galactoglucomannan That Maintains Pectin and Cellulose Architecture in Arabidopsis Seed Mucilage[1][OPEN]

Cătălin Voiniciuc*, Maximilian Heinrich-Wilhelm Schmidt, Adeline Berger, Bo Yang, Berit Ebert, Henrik V. Scheller, Helen M. North, Björn Usadel, and Markus Günl

Institute for Biosciences and Geosciences (Plant Sciences), Forschungszentrum Jülich, 52425 Juelich, Germany (C.V., M.H.-W.S., B.U., M.G.); Institute for Botany and Molecular Genetics, BioEconomy Science Center, RWTH Aachen University, 52056 Aachen, Germany (C.V., M.H.-W.S., B.Y., B.U.); Institut National de la Recherche Agronomique and AgroParisTech, Institut Jean-Pierre Bourgin, Unité Mixte de Recherche 1318, ERL Centre National de la Recherche Scientifique 3559, Saclay Plant Sciences, F–78026 Versailles, France (A.B., H.M.N.); Joint BioEnergy Institute and Physical Biosciences Division, Lawrence Berkeley National Laboratory, Berkeley, California 94702 (B.E., H.V.S.); and Department of Plant and Microbial Biology, University of California, Berkeley, California 94720 (H.V.S.)

ORCID IDs: 0000-0001-9105-014X (C.V.); 0000-0003-4576-6774 (M.H.-W.S.); 0000-0003-4446-0415 (B.Y.).

Plants invest a lot of their resources into the production of an extracellular matrix built of polysaccharides. While the composition of the cell wall is relatively well characterized, the functions of the individual polymers and the enzymes that catalyze their biosynthesis remain poorly understood. We exploited the Arabidopsis (*Arabidopsis thaliana*) seed coat epidermis (SCE) to study cell wall synthesis. SCE cells produce mucilage, a specialized secondary wall that is rich in pectin, at a precise stage of development. A coexpression search for *MUCILAGE-RELATED* (*MUCI*) genes identified *MUCI10* as a key determinant of mucilage properties. MUCI10 is closely related to a fenugreek (*Trigonella foenumgraecum*) enzyme that has in vitro galactomannan α-1,6-galactosyltransferase activity. Our detailed analysis of the *muci10* mutants demonstrates that mucilage contains highly branched galactoglucomannan (GGM) rather than unbranched glucomannan. MUCI10 likely decorates glucomannan, synthesized by CELLULOSE SYNTHASE-LIKE A2, with galactose residues in vivo. The degree of galactosylation is essential for the synthesis of the GGM backbone, the structure of cellulose, mucilage density, as well as the adherence of pectin. We propose that GGM scaffolds control mucilage architecture along with cellulosic rays and show that Arabidopsis SCE cells represent an excellent model in which to study the synthesis and function of GGM. Arabidopsis natural varieties with defects similar to *muci10* mutants may reveal additional genes involved in GGM synthesis. Since GGM is the most abundant hemicellulose in the secondary walls of gymnosperms, understanding its biosynthesis may facilitate improvements in the production of valuable commodities from softwoods.

[1] This work was supported by the Natural Sciences and Engineering Research Council of Canada (PGS–D3 grant to C.V.); by Saclay Plant Sciences (a travel grant to C.V.); by the Ministry of Innovation, Science, and Research of North-Rhine Westphalia (NRW), within the framework of the NRW Strategieprojekt BioSC (grant no. 313/323–400–00213 to M.H.-W.S. and B.U.); by the China Scholarship Council (grant no. 201206760005 to B.Y.); and by the U.S. Department of Energy, Office of Science, Office of Biological and Environmental Research (through contract DE–AC02-05CH11231 between the Lawrence Berkeley National Laboratory and the U.S. Department of Energy to B.E. and H.V.S.).

* Address correspondence to c.voiniciuc@fz-juelich.de.

The author responsible for distribution of materials integral to the findings presented in this article in accordance with the policy described in the Instructions for Authors (www.plantphysiol.org) is: Cătălin Voiniciuc (c.voiniciuc@fz-juelich.de).

C.V., B.U., and M.G. designed research; C.V. wrote the article, and B.U. and M.G. revised it; M.H.-W.S. performed cloning and *E. coli* work; A.B. and H.M.N. designed and performed immunolabeling experiments and electron microscopy; B.Y. performed CBM3a labeling and the Updegraff assay; B.E. and H.V.S. designed and performed *N. benthamiana* work; C.V. and M.G. performed the remaining experiments; all authors discussed the results and approved the final article.

[OPEN] Articles can be viewed without a subscription.

www.plantphysiol.org/cgi/doi/10.1104/pp.15.00851

The plant cell wall is the key determinant of plant growth (Cosgrove, 2005) and represents the most abundant source of biopolymers on the planet (Pauly and Keegstra, 2010). Consequently, plants invest a lot of their resources into the production of this extracellular structure. Thus, it is not surprising that approximately 15% of Arabidopsis (*Arabidopsis thaliana*) genes are likely dedicated to the biosynthesis and modification of cell wall polymers (Carpita et al., 2001). Plant walls consist mainly of polysaccharides (cellulose, hemicellulose, and pectin) but also contain lignin and glycoproteins. While the biochemical structure of each wall component has been relatively well characterized, the molecular players involved in their biogenesis remain poorly understood (Keegstra, 2010). The functions of the individual polymers, and how they are assembled into a three-dimensional matrix, are also largely unknown (Burton et al., 2010; Burton and Fincher, 2012).

Significant breakthroughs in cell wall research have been achieved through the examination of specialized plant tissues that contain elevated levels of a single

polysaccharide (Pauly and Keegstra, 2010). Some species, particularly legumes, accumulate large amounts of the hemicellulose galactomannan during secondary wall thickening of the seed (Srivastava and Kapoor, 2005). Analysis of the developing fenugreek (*Trigonella foenumgraecum*) endosperm led to the purification of a GALACTOMANNAN GALACTOSYLTRANSFERASE (TfGMGT), the first glycosyltransferase (GT) whose activity in plant cell wall synthesis was demonstrated in vitro (Scheller and Ulvskov, 2010). TfGMGT catalyzes the decoration of mannan chains with single α-1,6-galactosyl residues (Edwards et al., 1999). A similar approach in guar (*Cyamopsis tetragonoloba*) seeds revealed that the β-1,4-linked mannan backbone is synthesized by a member of the CELLULOSE SYNTHASE-LIKE A (CSLA) protein family (Dhugga et al., 2004).

Galactomannan functions as a storage polymer in the endosperm of the aforementioned seeds, analogous to starch in cereal grains (Dhugga et al., 2004), but it also has important rheological properties in the cell wall that have been exploited to produce valuable stabilizers and gelling agents for human consumption (Srivastava and Kapoor, 2005). The Man-to-Gal ratio is essential for the application of galactomannan gums in the food industry (Edwards et al., 1992). This is because unsubstituted mannan chains can interact via hydrogen bonds to produce crystalline microfibrils similar to cellulose (Millane and Hendrixson, 1994). Indeed, some algae that lack cellulose employ mannan fibrils as a structural material (Preston, 1968). The addition of Gal branches to the smooth, ribbon-like mannan chains creates hairy regions that limit self-association and promote gelation (Dea et al., 1977). All mannans are likely synthesized as highly substituted polymers that are trimmed in the cell wall (Scheller and Ulvskov, 2010).

Generally, polysaccharides containing backbones of β-1,4-linked Man units can be classified as heteromannan (HM). Galactoglucomannan (GGM) is the main hemicellulose in gymnosperm secondary walls and, in contrast to galactomannan, has a backbone that contains both Glc and Man units (Pauly et al., 2013). HM is detected in most Arabidopsis cell types (Handford et al., 2003) and facilitates embryogenesis (Goubet et al., 2009), germination (Rodríguez-Gacio et al., 2012), tip growth (Bernal et al., 2008), and vascular development (Benová-Kákosová et al., 2006; Yin et al., 2011). In the last 10 years, in vitro mannan synthase activity has been demonstrated for recombinant CSLA proteins from many land plants (Liepman et al., 2005, 2007; Suzuki et al., 2006; Gille et al., 2011; Wang et al., 2012). HM synthesis may also involve CELLULOSE SYNTHASE-LIKE D (CSLD) enzymes and MANNAN SYNTHESIS-RELATED (MSR) accessory proteins (Yin et al., 2011; Wang et al., 2013), but their precise roles in relation to the CSLAs have not been established. Arabidopsis CSLA2, like most other isoforms, can use both GDP-Man and GDP-Glc as substrates in vitro (Liepman et al., 2005, 2007) and is responsible for stem glucomannan synthesis in vivo along with CSLA3 and CSLA7 (Goubet et al., 2009). CSLA2 also participates in the synthesis of glucomannan present in mucilage produced by seed coat epidermal (SCE) cells (Yu et al., 2014).

Arabidopsis SCE cells represent an excellent genetic model in which to study the synthesis, polar secretion, and modification of polysaccharides, since these processes dominate a precise stage of seed coat development but are not essential for seed viability in laboratory conditions (Haughn and Western, 2012; North et al., 2014; Voiniciuc et al., 2015). Hydration of mature seeds in water releases a large gelatinous capsule, rich in the pectic polymer rhamnogalacturonan I, which can be easily stained or extracted (Macquet et al., 2007). Biochemical and cytological experiments indicate that Arabidopsis seed mucilage is more than just pectin and, in addition to cellulose, is likely to contain glycoproteins and at least two hemicellulosic polymers (Voiniciuc et al., 2015). There is mounting evidence that, despite their low abundance, these components play critical functions in seed mucilage architecture. The structure of homogalacturonan (HG), the major pectin in primary cell walls but a minor mucilage component, appears to be a key determinant of gelling properties and mucilage extrusion (Rautengarten et al., 2008; Saez-Aguayo et al., 2013; Voiniciuc et al., 2013). Mucilage attachment to seeds is maintained by the SALT OVERLY SENSITIVE5 glycoprotein and cellulose synthesized by multiple CELLULOSE SYNTHASE (CESA) isoforms (Harpaz-Saad et al., 2011; Mendu et al., 2011; Sullivan et al., 2011; Griffiths et al., 2014, 2015). From more than 35 genes that are reported to affect Arabidopsis seed mucilage properties (Voiniciuc et al., 2015), only *CSLA2*, *CESA3*, *CESA5*, *GALACTURONOSYLTRANSFERASE11* (*GAUT11*; Caffall et al., 2009), and *GAUT-LIKE5* (*GATL5*; Kong et al., 2013) are predicted to encode GTs. This highlights that, despite many detailed studies about mucilage production in SCE cells, the synthesis of its components remains poorly understood.

To address this issue, we conducted a reverse genetic search for *MUCILAGE-RELATED* (*MUCI*) genes that may be required for polysaccharide biosynthesis. One of these, *MUCI10*, encodes a member of the Carbohydrate Active Enzymes family, GT34 (Lombard et al., 2014), which includes at least two enzymatic activities and seven Arabidopsis proteins (Keegstra and Cavalier, 2010). Five of them function as XYLOGLUCAN XYLOSYLTRANSFERASES (XXT1–XXT5) in vivo and/or in vitro (Faik et al., 2002; Cavalier et al., 2008; Vuttipongchaikij et al., 2012). MUCI10/GT7 (At2g22900) and its paralog GT6 (At4g37690) do not function as XXTs (Vuttipongchaikij et al., 2012) and are more closely related to the TfGMGT enzyme (Faik et al., 2002; Keegstra and Cavalier, 2010). MUCI10, also called GALACTOSYLTRANSFERASE-LIKE6 (GTL6), served as a Golgi marker in multiple proteomic studies of Arabidopsis callus cultures (Dunkley et al., 2004, 2006; Nikolovski et al., 2012, 2014). Nevertheless, the role of TfGMGT orthologs in Arabidopsis remained unknown. We show that MUCI10 is responsible for the extensive galactosylation of glucomannan in mucilage and influences

glucomannan backbone synthesis, cellulose structure, and the distribution of pectin.

RESULTS

A *MUCI* Screen Yields a *TfGMGT* Ortholog

We used eight genes (At1g02720, At1g53500, At1g79840, At2g47670, At4g28370, At5g49360, At5g63800, and At5g67360), whose seed coat transcript levels are up-regulated during mucilage production (Voiniciuc et al., 2015), as baits in three distinct coexpression tools: GeneCAT, GeneMANIA, and ATTED-II (Mutwil et al., 2008; Warde-Farley et al., 2010; Obayashi et al., 2014). We manually prioritized a total of 600 *MUCI* gene predictions based on three criteria: putative protein function, seed coat expression profile, and the availability of insertion mutants. By screening more than 100 *muci* mutants for altered Ruthenium Red (RR) mucilage staining, we identified multiple new genes required for polysaccharide synthesis. This study focuses on *MUCI10*, and further results of the screen will be described elsewhere.

Both GeneCAT and GeneMANIA predicted that *MUCI10* is involved in mucilage polysaccharide production (Mutwil et al., 2008; Warde-Farley et al., 2010). Indeed, Arabidopsis microarray data sets indicate that *MUCI10* is closely linked to several known mucilage genes, particularly *CSLA2* (Fig. 1A). During seed development, *MUCI10* is specifically expressed in the seed coat, at the linear cotyledon and mature green embryo stages (Supplemental Fig. S1A; Winter et al., 2007; Belmonte et al., 2013). We validated this microarray data using reverse transcription (RT)-PCR (Fig. 1C) and quantitative reverse transcription (qRT)-PCR (Fig. 1D) analyses of *MUCI10* transcription in developing siliques. *MUCI10* expression increased from the heart to the linear cotyledon stage (Fig. 1, C and D) and peaked at the mature green embryo stage (Fig. 1D). *MUCI10* transcripts are 6.2 times more abundant in wild-type seed coats at 7 DPA (Supplemental Fig. S1B) compared with the *apetala2* (*ap2*) mutant, which does not produce mucilage (Dean et al., 2011). Similarly, *MUCI10* was expressed 5-fold lower when KNOTTED ARABIDOPSIS THALIANA7 (KNAT7) is disrupted (Fig. 1E). In contrast to its paralog, *GT6* does not classify as a *MUCI* gene, since it has 1.8 times higher expression in *ap2* than in the wild type (Supplemental Fig. S1C; Dean et al., 2011).

To investigate if *MUCI10* and *GT6* are involved in mucilage biosynthesis, we isolated four *muci10* and two *gt6* homozygous insertion mutants (Fig. 1B). The *muci10-1* and *muci10-2* alleles were shown to be transcriptional knockouts (Fig. 1, C and D). Since we detected increased *GT6* transcript levels in *muci10-2* siliques compared with the wild type (Fig. 1C), we generated a *muci10 gt6* double mutant to explore functional redundancy. The *muci10-2 gt6-1* double mutant only had traces of *GT6* transcript, similar to the *gt6-1* single mutant, not the elevated levels detected in the *muci10-2* single mutant (Fig. 1C).

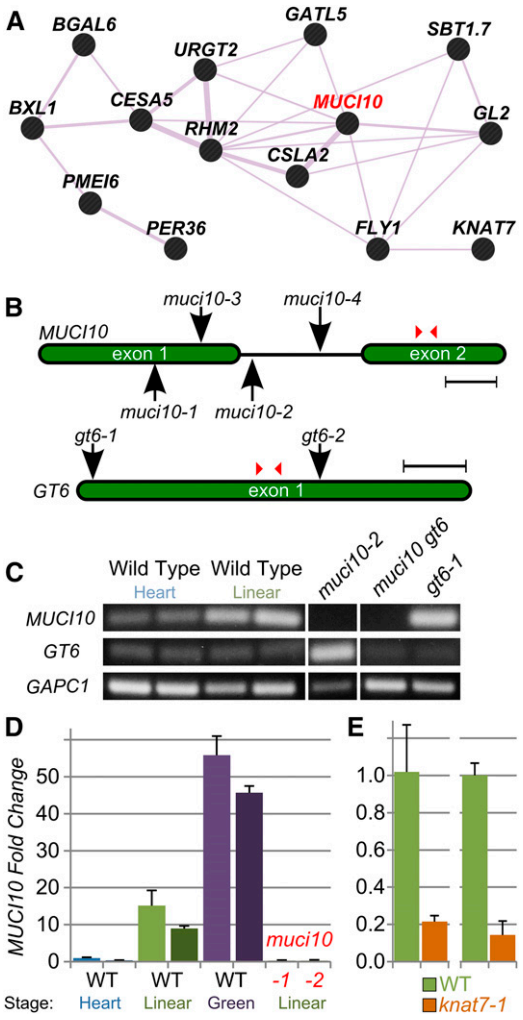

Figure 1. Analysis of the *MUCI10* gene and its paralog, *GT6*. A, *MUCI10* is coexpressed with known mucilage genes. Microarray data were visualized with GeneMANIA using all 14 genes as baits (Warde-Farley et al., 2010). B, *MUCI10* and *GT6* insertions and RT-PCR amplicons (red arrows). Bars = 200 bp. C to E, RT-PCR (C) and qRT-PCR (D and E) analyses of gene expression in siliques. Two wild-type (WT) biological replicates were tested at three stages of development (heart, linear cotyledon, and mature green), while all mutants were examined at the linear cotyledon stage. D and E, *MUCI10* expression (normalized to *UBIQUITIN5*) relative to the first wild type in each set. KNAT7 is a transcription factor predicted to promote hemicellulose biosynthesis in seed mucilage (Voiniciuc et al., 2015). Data show means + SD of four (D) or three (E) technical replicates.

Distinct *muci10* and *csla2* Chemical Defects Lead to Equally Compact Mucilage

The seeds of four independent *muci10* alleles were surrounded by smaller mucilage layers than the wild type (Fig. 2). Using Fiji (Schindelin et al., 2012), we developed a simple method that enables the

high-throughput quantification of seed and mucilage dimensions (Supplemental Fig. S2). Four *muci10* alleles and the *csla2-3* mutant, which has dense mucilage (Yu et al., 2014), displayed approximately 30% smaller mucilage capsules than the wild type (Fig. 2Q). Two *gt6* alleles showed normal mucilage dimensions, and the *muci10-2 gt6-1* double mutant resembled the *muci10-2* single mutant (Fig. 2). In contrast to their mucilage defects, all mutants had seed areas similar to the wild type (Supplemental Table S1), except for a 6% increase in *gt6-1* (Student's *t* test, $P < 0.05$). The equally compact mucilage capsules of *muci10* and *csla2* suggested that they may have similar chemical defects.

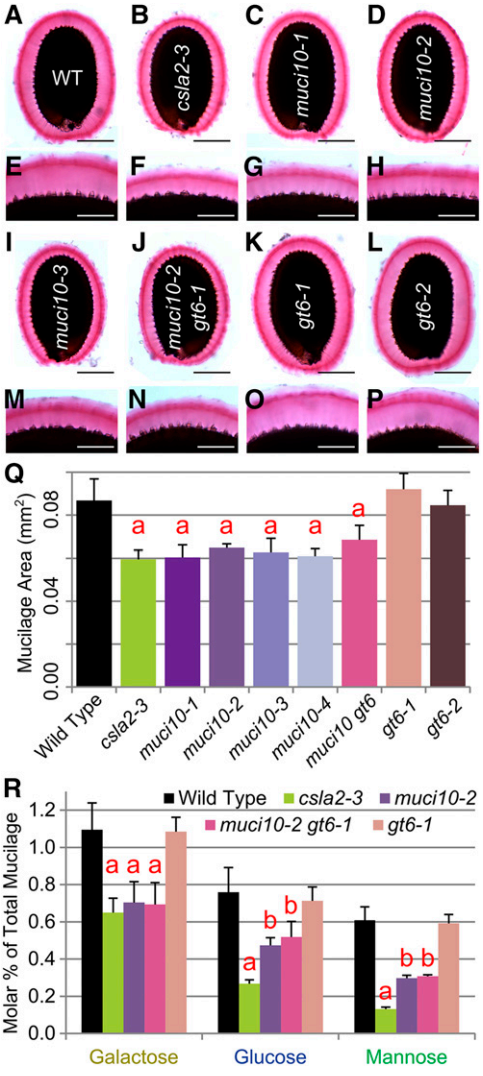

Figure 2. *muci10* and *csla2* have equally compact mucilage but distinct chemical defects. A to P, Pectin released from wild-type (WT) and mutant seeds was stained with RR. Bars = 200 μm (A–D and I–L) and 100 μm (E–H and M–P). Q, Area of RR-stained mucilage capsules. Data show means + SD of five biological replicates (more than 20 seeds each). R, Relative composition of total mucilage extracts. Data show means + SD of five biological replicates. The a indicates decreases relative to the wild type, while the b shows significant changes from the wild type and *csla2-3* (Student's *t* test, $P < 0.05$).

In mucilage extracted from these two mutants by vigorously shaking seeds in water (Voiniciuc et al., 2015), only three minor sugars (representing 2.5% of mucilage) were significantly altered from the wild type (Table I). The *muci10-2* and *csla2-3* mutants had equal reductions in Gal but contained distinct Glc and Man levels (Fig. 2R). The *csla2-3* mutant had approximately 80% less Man than wild-type mucilage (Table I), while the *muci10-1*, *muci10-2*, and *muci10-3* alleles only had approximately 50% less Man (Table I; Supplemental Tables S2 and S3). Given their identical staining and biochemical defects, the first two *muci10* lines were used interchangeably for further experiments. The changes in Gal, Glc, and Man content were proportional for each mutant (Fig. 2R). The *csla2-3* mutant lacked approximately 1 nmol of each of these three sugars per mg of seed, while *muci10-2* showed reductions of 0.9 nmol of Gal, 0.7 nmol of Glc, and 0.7 nmol of Man.

Unlike *MUCI10*, *GT6* Does Not Affect Seed Mucilage Composition

Unlike *muci10* mutants, *gt6-1* and *gt6-2* did not contain reduced Gal, Glc, or Man content in total mucilage (Table I; Fig. 2R) or nonadherent mucilage extracts (Supplemental Table S3). To test if *GT6* function can compensate partially for *MUCI10* function, we examined the biochemical composition of the *muci10-2 gt6-1* double mutant. The double mutant had a similar composition to the *muci10-2* mutant (Fig. 2R; Table I). This indicates that *GT6* is not indispensable for the synthesis of mucilage polysaccharides.

MUCI10 Is Necessary for GGM Synthesis

To further investigate *MUCI10* function, we analyzed the glycosyl linkages of total mucilage extracts (Table II) and used these results to calculate the composition of polysaccharides (Fig. 3A). While most polymers had wild-type levels, the *muci10-1* mucilage contained 38% less HM (Student's *t* test, $P < 0.05$). Unsubstituted glucomannan is the only known HM component of mucilage (Yu et al., 2014), although some of the available linkage data suggest the presence of GGM (Voiniciuc et al., 2015). Lower HM content in *muci10-1* mucilage resulted from reductions in terminal-Gal (t-Gal), 4-Glc, 4-Man, and 4,6-Man (Student's *t* test, $P < 0.05$), with 81% less t-Gal as the most severe defect (Table II; Fig. 3B). The loss of t-Gal correlated with a 5-fold decrease in the ratio of branched 4,6-Man to unbranched 4-Man (Fig. 3B). This indicates that *MUCI10* is required for the decoration of glucomannan with t-Gal side chains. Wild-type mucilage contained two branched 2,4-Man residues for every unbranched 4-Man unit (Table II), suggesting that GGM rather than unbranched glucomannan is the most abundant

Table I. *Monosaccharide composition of total mucilage extracts*

Relative monosaccharide composition (mol %) and total sugars (μg mg^{-1} seed) are shown in mucilage extracted by vigorous mixing in water. Values represent means ± SD of five biological replicates per genotype. Asterisks indicate significant differences (Student's *t* test, $P < 0.002$) from the wild type.

Sugar	Wild Type	*csla2-3*	*muci10-2*	*muci10-2 gt6-1*	*gt6-1*	*gt6-2*
Rha	44.12 ± 1.56	43.00 ± 1.82	43.33 ± 1.22	43.49 ± 2.24	41.64 ± 0.86	43.89 ± 1.53
Ara	0.93 ± 0.05	1.16 ± 0.10	1.11 ± 0.13	1.19 ± 0.18	0.98 ± 0.05	0.98 ± 0.02
Gal	1.10 ± 0.14	0.65 ± 0.08*	0.70 ± 0.11*	0.69 ± 0.12*	1.08 ± 0.08	1.01 ± 0.06
Glc	0.76 ± 0.13	0.33 ± 0.13*	0.47 ± 0.04*	0.52 ± 0.08	0.71 ± 0.07	0.69 ± 0.03
Xyl	3.11 ± 0.24	3.22 ± 0.10	3.30 ± 0.29	3.10 ± 0.16	3.15 ± 0.07	3.11 ± 0.15
Man	0.61 ± 0.07	0.13 ± 0.01*	0.30 ± 0.01*	0.31 ± 0.01*	0.59 ± 0.05	0.57 ± 0.03
GalA	49.21 ± 1.38	51.33 ± 1.72	50.62 ± 0.77	50.51 ± 1.70	51.69 ± 0.85	49.58 ± 1.71
Total	39.86 ± 3.24	38.35 ± 1.98	38.42 ± 3.85	43.51 ± 2.11	38.84 ± 1.82	39.58 ± 1.52

Man-containing polymer in mucilage. This model was also supported by an ELISA of total mucilage extracts using LM22 (Fig. 3C), a monoclonal antibody that only effectively binds HM polymers without Gal side chains (Marcus et al., 2010). Relative to wild-type mucilage, *muci10-1* contained significantly more non-galactosylated HM, while *csla2-3* contained significantly fewer LM22 epitopes (Fig. 3C). These results indicate that mucilage contains GGM, whose backbone is synthesized by CSLA2 and decorated by MUCI10, a putative α-1,6-galactosyltransferase (Fig. 3D). The presence of MUCI10 and/or galactosylation is also required for normal glucomannan backbone synthesis, since *muci10* mutants had 30% to 50% lower Glc and Man levels than the wild type (Figs. 2R and 3B). While GGM is primarily decorated with single α-1,6-Gal residues, *muci10-1* mucilage had significant reductions in both t-Gal and 2-Gal linkages (Fig. 3B). One out of every six 2,4-Man units might be substituted with β-1-2-Gal-α-1-6-Gal (Fig. 3D), a disaccharide found in GGM secreted by suspension-cultured tobacco (*Nicotiana tabacum* and *Nicotiana plumbaginifolia*) cells (Eda et al., 1985; Sims et al., 1997).

MUCI10 Is Essential for the Distribution of HM in Adherent Mucilage

To corroborate the biochemical changes detected in *csla2* and *muci10* mucilage extracts, we immunolabeled whole seeds with two monoclonal antibodies. INRA-RU1 binds unbranched rhamnogalacturonan I chains (Ralet et al., 2010), while LM21 binds effectively to all HM polymers, regardless of their degree of substitution (Marcus et al., 2010). Wild-type and mutant mucilage showed a similar INRA-RU1 labeling (Fig. 4, A–F), consistent with normal pectin synthesis. Mucilage LM21 signals could only be observed with a sensitive hybrid detector (Fig. 4, G–J), likely because GGM represents at most 2.5% of wild-type mucilage (Table I). LM21 labeled wild-type mucilage from the basal surface of columellae to the outer edge of the adherent mucilage capsule (Fig. 4G). However, LM21 signals were absent from ray-like regions above the columellae of wild-type (Fig. 4J) and *gt6-1* (Supplemental Fig. S3) seeds. Strikingly, no LM21 signals were detected in the mucilage capsules of *csla2-3*, *muci10-2* (Fig. 3), and *muci10-2 gt6-1* (Supplemental Fig. S3). Since these mutants contained 50% to 80% lower amounts of GGM sugars (Fig. 2R), LM21 epitopes might be reduced below the detection threshold.

GGM Is Required for the Synthesis and Distribution of Cellulose in Mucilage

As our *muci10-1* linkage data suggested a 45% decrease in cellulose (Student's *t* test, $P = 0.065$; Fig. 3A), which can be tightly associated with GGM (Eronen et al., 2011), we examined the structure of cellulose in mucilage using multiple probes and techniques. Pontamine Fast Scarlet 4B (S4B) is a cellulose-specific fluorescent dye (Anderson et al., 2010) and stained ray-like structures in wild-type mucilage (Fig. 5; Supplemental Fig. S4; Harpaz-Saad et al., 2011; Mendu et al., 2011; Griffiths et al., 2014). The *csla2-3* and *muci10*-2 mucilage capsules showed decreased S4B fluorescence compared with the wild type as well as a more compact cellulose distribution (Fig. 5), consistent with RR staining defects (Fig. 2). Surprisingly, these defects appeared to be as severe as in the *cesa5-1* cellulose mutant (Supplemental Fig. S4). Similar to S4B, *muci10-1* and *csla2-3* mucilage showed reduced staining with calcofluor, a β-glycan fluorescent dye (Fig. 6).

Despite decreased S4B and calcofluor staining, the mucilage capsules of GGM mutants were more readily labeled by CBM3a (Fig. 6; Supplemental Fig. S5), a carbohydrate-binding module that recognizes crystalline cellulose (Blake et al., 2006; Dagel et al., 2011). CBM3a epitopes were diffuse in wild-type mucilage but formed cap-like structures that topped *csla2-3* and *muci10-1* calcofluor-stained rays (Fig. 6, F and I). In contrast to the CBM3a labeling, the birefringence of crystalline cellulose in mucilage agreed with the S4B and calcofluor staining. Birefringent rays were equally reduced in three *muci10* alleles and *csla2-3* compared with the wild type (Fig. 7, A–E) but were entirely absent in the *cesa5-1* mutant (Fig. 7F), as reported previously (Sullivan et al., 2011). Consistent with the birefringence results, the seeds of GGM mutants contained intermediate amounts of crystalline cellulose compared with the wild type and *cesa5-1* (Fig. 7I). Therefore, *MUCI10* and

Table II. *Linkage analysis of total mucilage extracts*

Total mucilage was extracted by vigorous mixing in water. Values represent the relative composition (mol %) of each linkage ± SD of three biological replicates. Asterisks indicate significant differences (Student's *t* test, $P < 0.05$) from the wild type.

Linkage	Wild Type	*muci10-1*
Rha		
t-Rha	0.49 ± 0.19	0.31 ± 0.19
2-Rha	36.81 ± 0.38	36.69 ± 3.30
2,3-Rha	0.66 ± 0.11	0.86 ± 0.42
2,4-Rha	0.85 ± 0.24	1.31 ± 1.15
Ara		
t-Ara	0.07 ± 0.03	0.06 ± 0.01
3-Ara	0.41 ± 0.04	0.74 ± 0.29
5-Ara	0.19 ± 0.04	0.23 ± 0.03
Gal		
t-Gal	0.71 ± 0.09	0.13 ± 0.05*
2-Gal	0.11 ± 0.01	0.03 ± 0.02*
4-Gal	0.11 ± 0.00	0.11 ± 0.04
6-Gal	0.21 ± 0.11	0.17 ± 0.07
2,4-Gal	0.08 ± 0.01	0.08 ± 0.04
4,6-Gal	0.05 ± 0.03	0.03 ± 0.02
3,6-Gal	0.29 ± 0.05	0.55 ± 0.39
Glc		
t-Glc	0.01 ± 0.01	0.00 ± 0.00
4-Glc	1.07 ± 0.03	0.73 ± 0.10*
3,4-Glc	0.01 ± 0.01	0.02 ± 0.00
4,6-Glc	0.07 ± 0.01	0.06 ± 0.02
Xyl		
t-Xyl	0.43 ± 0.05	0.42 ± 0.06
4-Xyl	1.61 ± 0.11	1.60 ± 0.04
2,4-Xyl	1.33 ± 0.04	1.45 ± 0.12
Man		
4-Man	0.25 ± 0.01	0.34 ± 0.03*
4,6-Man	0.53 ± 0.12	0.14 ± 0.09*
GalUA		
t-GalA	0.80 ± 0.33	0.56 ± 0.23
4-GalA	51.39 ± 0.66	50.78 ± 0.57
2,4-GalA	0.56 ± 0.11	0.73 ± 0.36
4,6-GalA	1.24 ± 0.16	1.80 ± 1.21

CSLA2 are not only required for the synthesis of GGM in seed coat epidermal cells but also maintain the structure of cellulose in mucilage.

Cellulose and GGM Are Both Required for Mucilage Attachment to Seeds

Reduced cellulose synthesis in *cesa5* mutants causes severe mucilage detachment from seeds (Harpaz-Saad et al., 2011; Mendu et al., 2011; Sullivan et al., 2011). The *muci10-2* mutant had more nonadherent mucilage than the wild type but significantly less than *cesa5-1* (Fig. 7J). Polymers containing Man were particularly easy to detach from *muci10-2*. Since *muci10-2* had wild-type levels of total mucilage sugars (Table I) and only an 8% overall reduction in their adherence, its 25% smaller RR-stained capsule may also result from the increased compactness of adherent polysaccharides (Fig. 2Q).

Previously, *csla2-1* mucilage capsules were easily digested by an endo-β-1,4-glucanase from *Aspergillus niger* (Yu et al., 2014). A 90-min treatment with a similar β-glucanase, purified from *Trichoderma longibrachiatum*, fully detached *csla2-3* and *muci10-1* adherent mucilage but had minor effects on the wild type (Supplemental Fig. S6). The *muci10-1* seeds had clear mucilage detachment after only a 50-min β-glucanase digestion (Fig. 8), showing that cell wall architecture was weakened by the loss of GGM and that endo-1,4-β-D-glucanase (β-Glc) linkages maintain mucilage adherence. While β-Glc linkages are typically derived from cellulose, they also form GGM along with α-galactosidase (α-Gal) and endo-1,4-β-mannanase (β-Man) linkages (Fig. 3D).

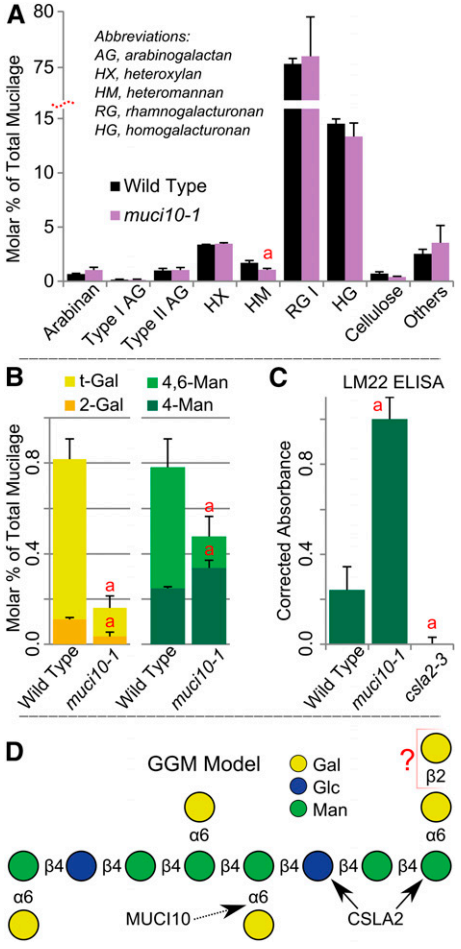

Figure 3. Polysaccharide structure in wild-type and *muci10* total mucilage extracts. A, Polysaccharide abundance calculated based on the linkage analysis in Table II. B, The frequency of Gal and Man linkages is altered in *muci10-1* mucilage. C, Quantification of nongalactosylated HM, relative to *csla2-3* mucilage, using the LM22 antibody (Marcus et al., 2010). Data show means + SD of three biological replicates, except two replicates for the wild type and *muci10-1* in C. The a indicates a significant change from the wild type (Student's *t* test, $P < 0.05$). D, Model of GGM in wild-type mucilage, showing likely roles of CSLA2, a glucomannan synthase, and MUCI10, a putative α-1,6-galactosyltransferase. Mucilage GGM may also contain a rare β-1,2-Gal residue, added by an unknown enzyme.

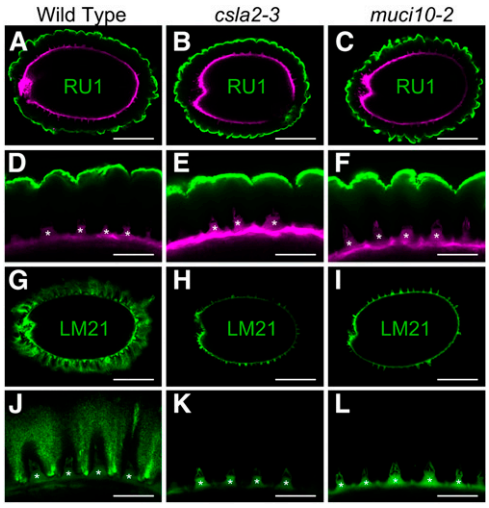

Figure 4. Immunolabeling of pectin and HM in extruded mucilage. INRA-RU1 labeled rhamnogalacturonan I RG I (A–F), and LM21 labeled HM (G–L). Each image shows an optical section through a whole seed (green = antibody and magenta = seed intrinsic fluorescence). Asterisks indicate columellae. Bars = 200 μm (A–C and G–I) and 50 μm (D–F and J–L).

To test if GGM itself mediates adherence, we digested mucilage with α-galactosidase and/or β-mannanase, two *A. niger* enzymes that exhibit synergistic degradation of galactomannan (Manzanares et al., 1998). Compared with the buffer control, single-enzyme treatments slightly enlarged the mucilage capsules and obscured the RR staining differences between the wild type and *muci10-1* (Fig. 8). Counterstaining revealed that the cellulosic dye S4B could not penetrate RR-stained adherent mucilage capsules (Fig. 9, A–C). Strikingly, wild-type and *muci10-1* seeds digested with both α-galactosidase and β-mannanase were surrounded by S4B-stained cellulosic rays (Fig. 9, D–I) but no RR-stained pectin (Fig. 8, M and N). The digested *muci10-1* seeds had reduced S4B fluorescence compared with the wild type (Fig. 9, E and H), similar to *muci10-2* intact mucilage capsules (Fig. 5; Supplemental Fig. S4). The digested seeds also displayed disc-like structures visible with transmitted light and stained by S4B (Fig. 9, D–I), resembling the detached primary cell walls of the *fly1* mutant (Voiniciuc et al., 2013). These results suggest that polymers containing α-Gal and β-Man linkages, namely GGM, are required for the adherence of pectin to Arabidopsis seeds.

MUCI10 Controls Mucilage Density Independently of Calcium Cross Links

Dextran molecules labeled with fluorescein isothiocyanate (FITC) can be used to examine mucilage porosity (Willats et al., 2001). While 4- and 20-kD FITC-dextrans reached the seed surface, 40-kD molecules were excluded from thin rays in the wild type and were absent from wide mucilage columns in *muci10-1* and *muci10-2* (Supplemental Fig. S7). Accordingly, 70-kD FITC-dextrans were largely absent from *muci10* and *csla2-3* mucilage but only partially excluded from rays in the wild type (Fig. 10, A–D). In *cesa5-1*, which retains cellulosic rays despite reduced adherent mucilage (Supplemental Fig. S4), 70-kD molecules reached the seed surface (Fig. 10F). Therefore, *muci10* mutants not only had an increase in mucilage detachment but also had a denser mucilage capsule formed by the adherent polysaccharides.

Since the compactness of *csla2-1* was suggested to result from increased calcium cross links in mucilage (Yu et al., 2014), we investigated how calcium ions affect *muci10* staining defects (Fig. 10, G–L) by treating seeds with $CaCl_2$ and EDTA, a divalent cation chelator. $CaCl_2$ treatment prevents mucilage extrusion from mutants that can form more HG cross links (Voiniciuc et al., 2013) but did not impair *muci10* mucilage release (Fig. 10K). EDTA rescues mucilage defects caused by increased calcium cross links (Rautengarten et al., 2008; Saez-Aguayo et al., 2013; Voiniciuc et al., 2013) but did not expand the *muci10* mucilage capsule (Fig. 10L) to the wild-type level (Fig. 10I). Since *muci10* mucilage was more compact than wild-type mucilage regardless of the presence of calcium, the denser mucilage is most likely the direct result of decreases in GGM rather than increased HG cross links.

The *muci10* Mutant Only Shows Major Defects in Seed Mucilage Architecture

To explore if the function of *MUCI10* extends beyond the mucilage of SCE cells and to elucidate the role of *GT6*, we examined their mutant phenotypes in other cell walls. The dry seed surface morphology of all the mutants examined, including *muci10 gt6*, was similar to the wild type with scanning electron microscopy (Supplemental Fig. S8). No clear differences in SCE cell

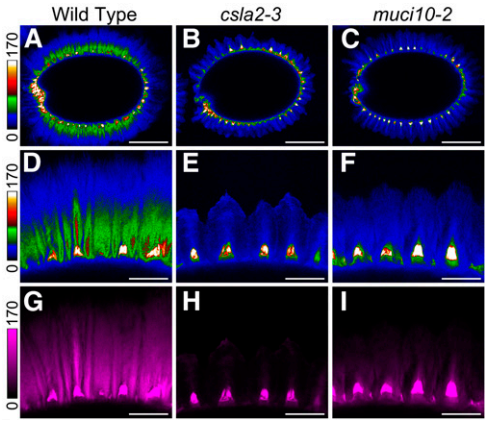

Figure 5. Mutants with GGM defects display reduced S4B labeling of cellulose. Cellulose distribution is shown in wild-type, *csla2-3*, and *muci10-2* mucilage extruded from seeds hydrated in water. S4B signal intensity was visualized with the Thal look-up table in Fiji (A–F) or as magenta (G–I). Bars = 200 μm (A–C) and 50 μm (D–I).

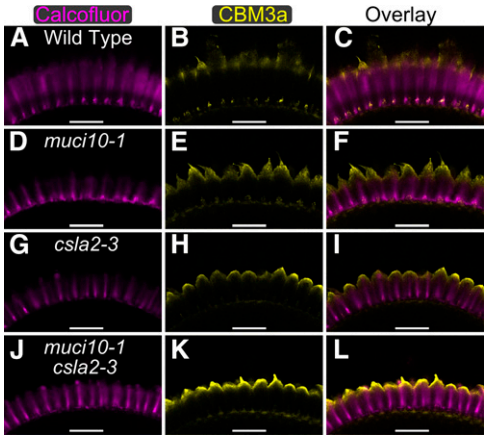

Figure 6. Impaired GGM structure alters cellulose and β-glycan distribution in mucilage. Mucilage was immunolabeled with CBM3a (yellow), which has high affinity for crystalline cellulose. β-Glycans were then stained with calcofluor (magenta). Bars = 100 μm.

shape or size were detected. Since *GT6* may be expressed in subepidermal seed coat layers (Supplemental Fig. S1C), we analyzed the distribution of HM epitopes labeled by LM21 in cryosections of *muci10-2*, *gt6-1*, and *muci10-2 gt6-1* mature seeds (Supplemental Fig. S9). Similar to the whole-mount immunolabeling of adherent mucilage (Fig. 4; Supplemental Fig. S3), LM21 epitopes surrounded wild-type and *gt6-1* columellae (Supplemental Fig. S9). The analysis of cryosectioned seeds did not reveal any clear defects in other cell walls of the seed, suggesting that *MUCI10* specifically affects GGM synthesis in SCE cells. Accordingly, *muci10* and *gt6* single and double mutants were morphologically similar to wild-type plants throughout development. While CSLA2 and related isoforms are required for the synthesis of HM in stems (Goubet et al., 2009), *MUCI10* and *GT6* did not affect the cell wall composition of this tissue (Supplemental Fig. S10), consistent with unbranched glucomannan representing the main HM in Arabidopsis stems (Goubet et al., 2009).

MUCI10 Is Localized in the Golgi

MUCI10 tagged with sYFP, a yellow super fluorescent protein (Kremers et al., 2006), localized to small punctae in Arabidopsis cells, while the sYFP tag alone was diffused in the cytosol (Fig. 11, A and B). The small punctae of both MUCI10-sYFP and Wave22Y, a Golgi marker (Geldner et al., 2009), aggregated into large compartments (Fig. 11, C–F) after cells were treated with brefeldin A, an inhibitor of secretion (Nebenführ et al., 2002). In addition, MUCI10-sYFP proteins colocalized with the Golgi marker sialyltransferase (ST)-RFP (Teh and Moore, 2007) when stably expressed in Arabidopsis leaf epidermal cells (Fig. 11, G–I). These results are consistent with MUCI10/GTL6 serving as a Golgi marker in multiple proteomic studies (Dunkley et al., 2004, 2006; Nikolovski et al., 2012, 2014).

The Degree of Galactosylation Is Critical for GGM Synthesis and Mucilage Properties

We isolated four independent *muci10-1 35S:MUCI10-sYFP* T1 plants, which displayed small fluorescent punctae (Fig. 11). Analysis of total mucilage extracts from the resulting seeds showed that the MUCI10-sYFP proteins could at least partially complement the reduced GGM sugar content of *muci10-1*, unlike the *35S:sYFP* control (Fig. 12A). While all four *muci10-1* complemented lines had fully rescued levels of Glc and Man, only line 1 had a degree of galactosylation that was close to the wild-type mucilage. The other three lines had intermediate Gal levels (Fig. 12A) and displayed equally compact mucilage capsules to the *muci10-1* and *muci10-1 35S-sYFP* seeds (Fig. 12J). Interestingly, line 1 had large RR-stained mucilage capsules,

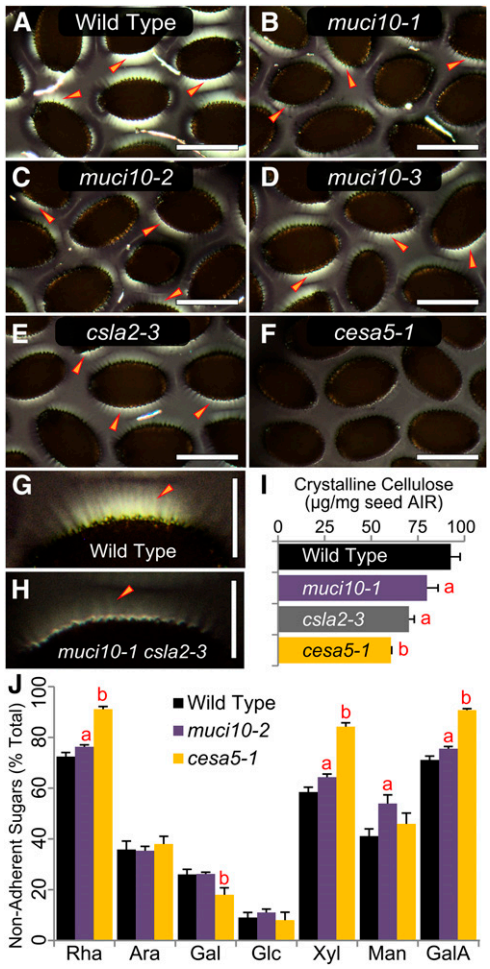

Figure 7. *MUCI10* partly controls crystalline cellulose levels and mucilage adherence. A to H, Birefringence (arrowheads) of crystalline cellulose in mucilage. Bars = 0.5 mm (A–F) and 0.2 mm (G and H). I, Seed crystalline cellulose quantified with the Updegraff assay. J, Percentage of each mucilage sugar that is nonadherent. Data show means + SD of three biological replicates (I and J). Letters indicate changes from the wild type (Student's *t* test, $P < 0.05$).

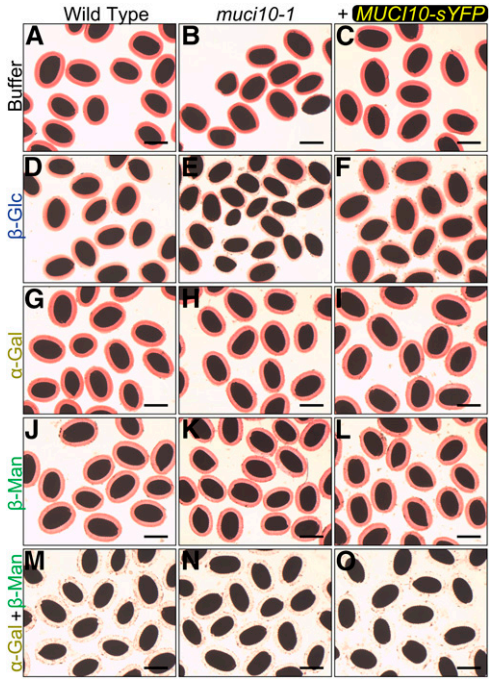

Figure 8. β-Glc, α-Gal, and β-Man linkages are required for seed mucilage attachment. RR staining of pectin is shown after β-Glc, α-Gal, and/or β-Man enzymatic digestions (50 min, 40°C, and pH 4.5). The images at right show that *35S:MUCI10-sYFP* (line 1) rescues the sensitivity of *muci10-1* to β-Glc digestion. Discs remain around seeds only after α-Gal and β-Man double digestion (M–O). Bars = 1 mm.

similar in size to the wild type (Fig. 12, B–J). This complemented line also resembled the wild type after enzymatic digestion (Fig. 8) and in the 70-kD FITC-dextran experiment (Fig. 10). Since line 1 only differed from the other T1 lines by its high Gal content, the precise degree of GGM substitution may be essential for mucilage properties.

MUCI10 Is Required for the Extensive Decoration of Glucomannan Synthesized by CSLA2

To validate that *MUCI10* functions downstream of *CSLA2* in the synthesis of GGM (Fig. 3D), we isolated a *muci10-1 csla2-3* homozygous double mutant. This double mutant resembled the *csla2-3* single mutant in our analysis of RR staining (Fig. 12E), mucilage area (Fig. 12J), cellulose birefringence (Fig. 7H), and CBM3a labeling (Fig. 6, J–L; Supplemental Fig. S5, J–L). Furthermore, the *35S:MUCI10-sYFP* transgene could not complement *csla2-3* (Fig. 12I), consistent with the *csla2-3* mutation being epistatic to *muci10-1* (Fig. 3D). Although MUCI10 and its paralog likely function as α-1, 6-galactosyltransferases, we could not confirm this activity in vitro. GLUTATHIONE *S*-TRANSFERASE (GST)-tagged soluble MUCI10 and GT6 proteins purified from *Escherichia coli* were unable to add Gal to available mannan or glucomannan substrates (Supplemental Fig. S11). Similarly, *Nicotiana benthamiana* microsomes containing full-length MUCI10 proteins tagged with YFP did not show any incorporation of [^{14}C]Gal into mannohexaose relative to controls.

CSLA2 and *MUCI10* Might Not Be Sufficient for GGM Synthesis

Via an independent screen, we identified multiple natural accessions with mucilage defects similar to the *muci10* and *csla2* insertion mutants. Lm-2 (Le Mans, France), Ri-0 (Richmond, British Columbia, Canada), and Lc-0 (Loch Ness, Scotland, United Kingdom) lacked the HM epitopes recognized by LM21 in Columbia-0 wild-type mucilage (Supplemental Fig. S3) but had normal dry seed surface morphology (Supplemental Fig. S8). According to the Arabidopsis 1001 Genomes project (http://signal.salk.edu/atg1001/3.0/gebrowser.php; Cao et al., 2011), these natural accessions do not have unique mutations in the *CSLA2* or *MUCI10* coding regions. This could indicate that additional genes required for HM synthesis are mutated in the natural accessions.

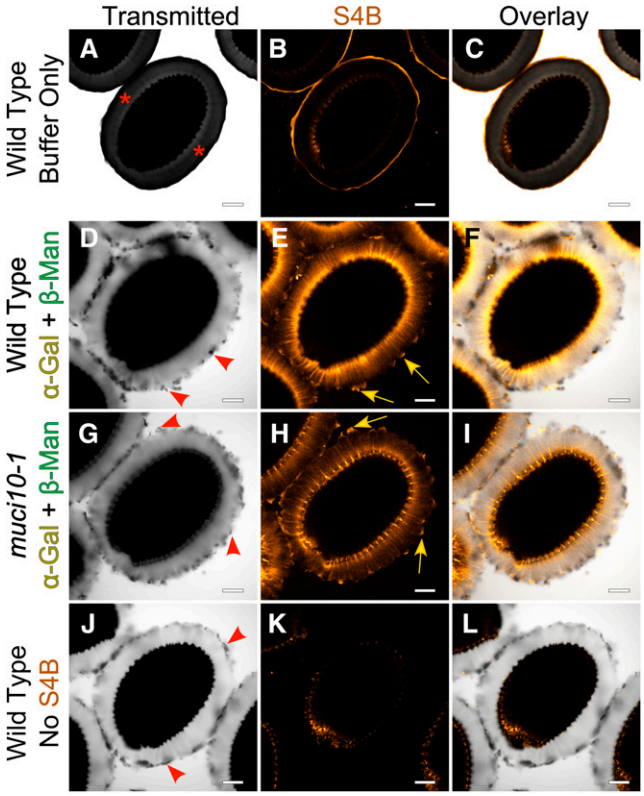

Figure 9. α-Gal and β-Man linkages primarily maintain the adherence of pectin, not cellulose. After digestion of α-Gal and β-Man linkages in mucilage, pectin was stained with RR (see Fig. 8) and cellulose was counterstained with S4B. Asterisks show that S4B cannot penetrate RR-stained adherent mucilage and only stained cellulosic rays when pectin was detached. Discs visible with light (arrowheads) were labeled by S4B (arrows). Bars = 100 μm.

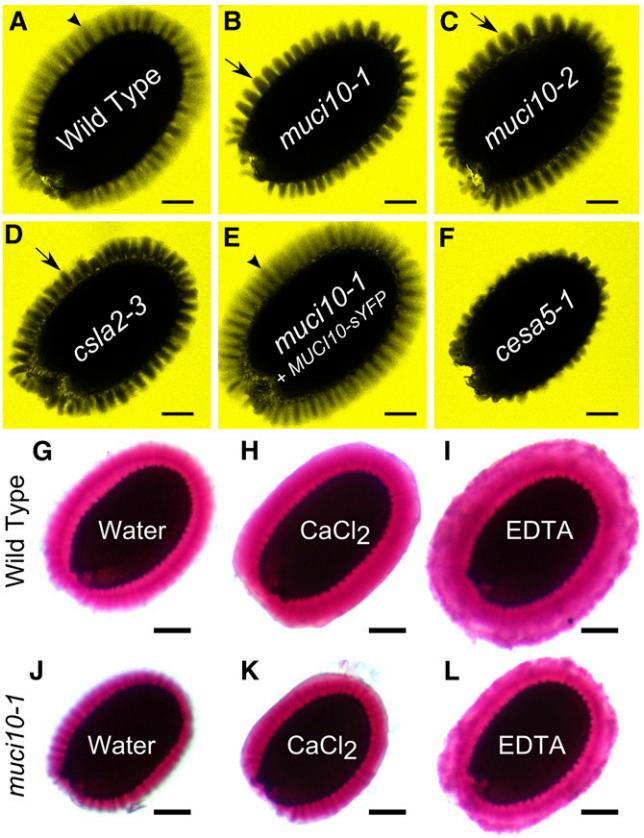

Figure 10. *MUCI10* controls mucilage density independently of calcium cross-links. A to F, FITC-dextran 70-kD molecules (yellow) were excluded from thin rays (arrowheads) or wide mucilage columns (arrows) but fully penetrated *cesa5-1* mucilage (F). G to L, The *muci10-1* seeds released more compact mucilage than the wild type when imbibed in water, $CaCl_2$, or EDTA for 60 min before rinsing with water and staining with RR. Bars = 100 μm.

DISCUSSION

Although Arabidopsis seed mucilage has been exploited for more than a decade to study cell wall production, only a few enzymes directly required for polysaccharide synthesis in SCE cells have been identified so far (Voiniciuc et al., 2015). To tackle this problem, we conducted a reverse genetic screen for *MUCI* genes that has predicted many glycosyltransferases. Using eight gene baits in multiple coexpression tools, we generated a more comprehensive set of candidate genes for cell wall biosynthesis than previous approaches that used only one or two baits (Vasilevski et al., 2012; Ben-Tov et al., 2015). *MUCI10*, the first of these genes to be characterized in detail, encodes a putative α-1,6-galactosyltransferase related to the fenugreek TfGMGT enzyme that decorates mannan chains with t-Gal residues (Edwards et al., 1999). As suggested by the public microarray data and qRT-PCR analysis (Fig. 1, D and E), *MUCI10* is required for mucilage synthesis during seed coat development. *MUCI10* facilitates the extensive galactosylation of glucomannan in mucilage, a role consistent with a functional paralog of *TfGMGT*. *GT6*, the closest paralog of *MUCI10*, is also expressed in seeds, but its transcriptional profile is not consistent with mucilage production (Supplemental Fig. S1). Indeed, *gt6* mutants and a *muci10 gt6* double mutant indicate that *GT6* is not critical for mucilage structure.

MUCI10 Enables the Synthesis of Highly Galactosylated Glucomannan in Mucilage

Mutations in *MUCI10* primarily disrupted HM synthesis in mucilage (Figs. 3A and 4). Our detailed characterization of *muci10* mutants and reanalysis of *csla2-3* revealed that GGM represents at least 80% of Man-containing

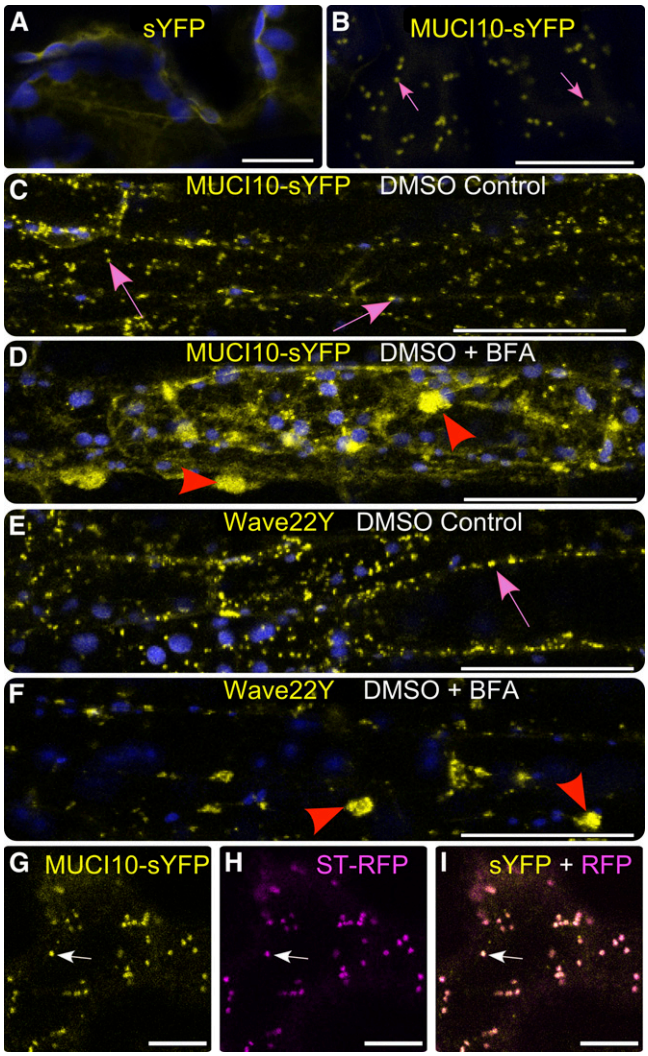

Figure 11. MUCI10-sYFP punctae are sensitive to brefeldin A (BFA) and colocalize with ST-RFP. Fluorescent proteins were stably expressed in Arabidopsis leaf (A, B, and G–I) and hypocotyl (C–F) epidermal cells. Images show one (A, B, and G–I) or three (C–F; Z-project, maximum intensity method) optical slices and intrinsic chloroplast fluorescence (blue). Wave22Y and ST-RFP are Golgi markers. Arrows show punctae, and arrowheads mark large brefeldin A compartments. Bars = 20 μm (A and B), 50 μm (C–F), and 10 μm (G–I).

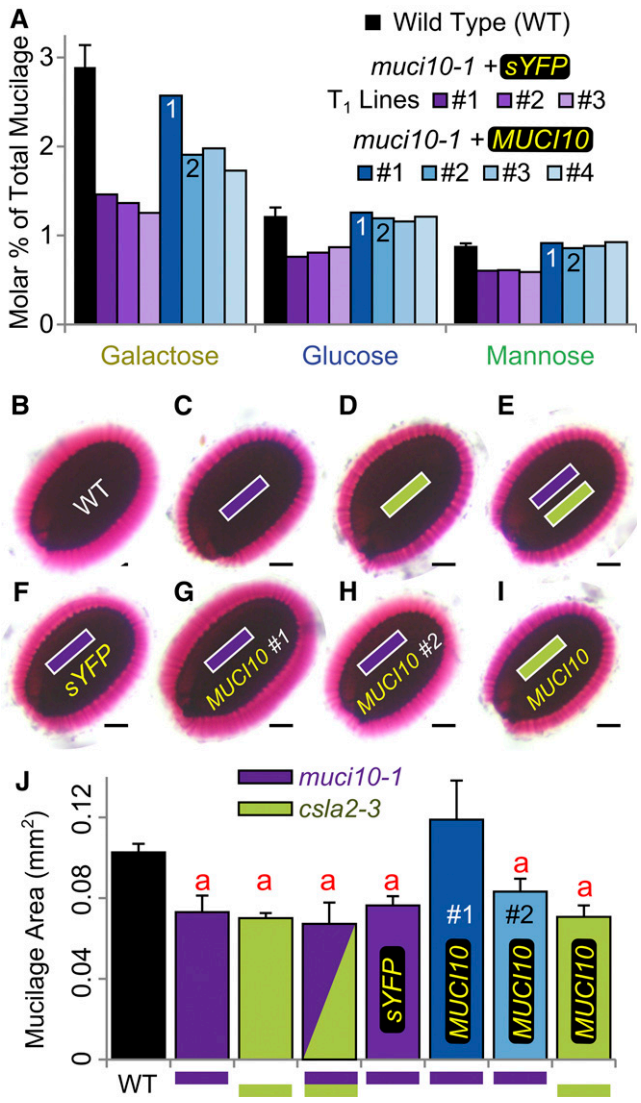

Figure 12. MUCI10 enables galactosylation of glucomannan synthesized by CSLA2. A, YFP-tagged MUCI10 at least partially rescued GGM synthesis in four independent *muci10-1* T1 lines. Only MUCI10 line 1 had Gal content (A), RR staining, and mucilage area similar to the wild type (WT; B–J). In B to J, colors denote plants homozygous for *muci10-1* (purple) and/or *csla2-3* (green) mutations. Error bars indicate SD of three biological or technical (only for lines 1 and 2 and *muci10 csla2*) replicates. The a indicates changes from the wild type (Student's *t* test, $P < 0.05$). Bars = 100 μm.

polymers in Arabidopsis seed mucilage. The initial study of *csla2* mucilage focused exclusively on glucomannan (Yu et al., 2014) and most likely underestimated the abundance of HM in mucilage and its degree of branching. In our linkage analysis (Table II), wild-type mucilage contained two branched 2,4-Man residues for every unbranched 4-Man unit, consistent with the presence of highly branched GGM rather than unbranched glucomannan. While four independent *muci10* insertion mutants and *csla2-3* displayed equally compact mucilage capsules compared with wild-type seeds (Fig. 2Q), biochemical analysis revealed distinct underlying defects (Fig. 2R). Consistent with CSLA2 synthesizing the backbone of GGM (Fig. 3D), its absence resulted in a significant loss of Gal, Glc, and Man residues in mucilage, almost in a 1:1:1 molar ratio (Table I). In contrast, *muci10* mutants had a unique biochemical defect, with significantly greater reductions of Gal compared with Glc and Man (Fig. 2R). The *muci10-1* knockout mutant had 81% less t-Gal, a 5-fold lower ratio of branched 4,6-Man to unbranched 4-Man (Fig. 3B; Table II), and a 4-fold increase in LM22 epitopes (Fig. 3C) relative to the wild type. Since the LM22 antibody only effectively binds nongalactosylated HM (Marcus et al., 2010), wild-type mucilage contained highly branched HM, while *muci10* mutants had an exceptionally low degree of HM galactosylation.

Our phenotypic analysis of *muci10-1 35S:MUCI10-sYFP* lines indicates that the degree of galactosylation is of paramount importance for the functions of GGM in mucilage (Fig. 12). The addition of some Gal side chains and/or the presence of MUCI10 in a protein complex appear to be essential for the normal synthesis of the GGM backbone by CSLA2, since *muci10* mutants have lower Glc and Man levels (Figs. 2R and 3B). Indeed, all HM polymers are likely synthesized in a highly galactosylated form in the Golgi (Scheller and Ulvskov, 2010). An intermediate Gal level in three independent transformants was sufficient to rescue the GGM backbone sugars to the wild-type level but was not high enough to rescue the compact mucilage defect (Fig. 12). The *muci10 csla2* double mutant supports the model proposed in Figure 3D, since it resembled the *csla2* single mutant in our analysis of pectin (Fig. 12) and cellulose (Figs. 6 and 7) structures. Furthermore, the *35S:MUCI10-sYFP* transgene could not complement the *csla2* mutant (Fig. 12), consistent with *MUCI10* functioning downstream of *CSLA2* in the synthesis of GGM.

MUCI10 Is Critical for the Organization of Seed Mucilage Polysaccharides

The loss of highly substituted GGM in *muci10* is associated with smaller mucilage capsules. This phenotype is best explained by the partial detachment of certain polysaccharides and an increased density of the polymers that remain attached to the seed. Since Man-containing polymers were particularly easy to detach from *muci10* (Fig. 7J), HM with a low degree of galactosylation might be less adherent and could explain the lack of LM21 epitopes in *muci10* and *csla2* adherent mucilage capsules (Fig. 4). The 8% increased detachment of *muci10* mucilage only partially explains the approximately 30% smaller capsules. FITC-dextran experiments indicate that molecules above 20 kD are preferentially excluded from *muci10* and *csla2-3* mucilage capsules, consistent with the increased density of the adherent polysaccharides (Fig. 10; Supplemental Fig. S7). Although the denser *csla2* mucilage was proposed to result from increased calcium cross links (Yu et al., 2014), *muci10* capsules were more compact than

wild-type capsules, regardless of the presence or absence of calcium ions (Fig. 10).

Our analysis of single and double mutants shows that GGM synthesized by CSLA2 and MUCI10 maintains the structure of cellulose in seed mucilage. GGM mutants had decreased calcofluor and S4B staining of cellulose, reduced birefringence, and less crystalline cellulose in seeds (Figs. 5–7) but were usually less severe than the *cesa5-1* mutant. CBM3a labeled cap-like structures around *muci10-1* and *csla2-3* single and double mutant seeds, consistent with a previous study (Yu et al., 2014). As discussed in a recent review (Voiniciuc et al., 2015), CBM3a specificity and/or accessibility is puzzling. The *cesa5* (Sullivan et al., 2011; this study), *csla2* (Yu et al., 2014; this study), and *muci10* (this study) mucilage had increased CBM3a labeling, despite clear decreases in cellulose content via other probes and techniques.

GGM Scaffolds and Cellulosic Rays Maintain the Architecture of Mucilage

Two distinct structures, which partially overlap, are likely to control mucilage architecture. SCE cells release cellulosic rays that extend above columellae and anchor mucilage polymers to the seed (Fig. 5; Supplemental Fig. S4; Harpaz-Saad et al., 2011; Mendu et al., 2011; Sullivan et al., 2011; Griffiths et al., 2014, 2015). We propose that a GGM scaffold surrounds the cellulosic rays in the mucilage capsule (Fig. 4J) and controls the spacing of mucilage polymers. GGM can form tight associations with cellulose (Eronen et al., 2011), but its Gal side chains can generate hairy regions that promote gelation (Dea et al., 1977). While the cellulosic ray is indispensable for adherence, highly branched GGM scaffolds primarily control mucilage density. Reduced galactosylation may cause the GGM scaffolds to flatten and the surrounding polymers to either detach from the seed or be more tightly packed in the adherent mucilage capsule.

Consistent with this model, *muci10* and *csla2* had compromised mucilage architecture and were more susceptible to β-glucanase digestion than the wild type (Fig. 8; Supplemental Fig. S6). β-Glc linkages, primarily from cellulose, are essential for the adherence of mucilage polysaccharides. Using *A. niger* α-galactosidase and β-mannanase, which synergistically degrade galactomannan (Manzanares et al., 1998), we demonstrated that polymers containing α-Gal and β-Man linkages, mainly GGM, are also required for the adherence of pectin, but not cellulose, to the seed (Figs. 8 and 9). This further supports the role of GGM as a scaffold that maintains the distribution of pectic polysaccharides.

MUCI10 Is Essential, But Not Sufficient, for GGM Synthesis

CSLA2 and MUCI10 are Golgi-localized proteins (Fig. 11; Nikolovski et al., 2014; Yu et al., 2014) and are likely the key enzymes required for GGM synthesis in the Golgi apparatus. Although we did not detect in vitro galactosyltransferase activity for MUCI10 recombinant proteins purified from *E. coli* or expressed in *N. benthamiana* microsomes, only a few plant glycosyltransferases have been biochemically characterized through direct assays. Such enzymes are typically highly unstable membrane-bound proteins (Brown et al., 2012). However, MUCI10-sYFP could fully complement the biochemical defects and altered properties of the *muci10-1* mutant. Consistent with MUCI10 substituting glucomannan synthesized by CSLA2, the MUCI10-sYFP protein could not rescue the *csla2* mucilage defects.

The lack of MUCI10 in vitro activity may indicate that GGM synthesis requires a protein complex. The synthesis of xyloglucan, another hemicellulose, requires homocomplexes and heterocomplexes of CSLC4, a β-1,4-glucan synthase (Cocuron et al., 2007), and XXT proteins (Chou et al., 2012, 2015). Since CSLA2 and MUCI10 are members of the same GT families as CSLC4 and XXTs, respectively, future studies should investigate if similar protein-protein interactions facilitate GGM synthesis. Indeed, two proteins (MSR1 and MSR2) were already proposed to promote glucomannan synthesis by stabilizing CSLA enzymes (Wang et al., 2013). An alternative possibility is that MUCI10 requires glucomannan acceptors, in contrast to the fenugreek TfGMGT enzyme, which uses pure mannooligosaccharides with a length of at least five units (Edwards et al., 1999). This could not be fully tested due to the limited availability of glucomannan acceptor substrates. Although purified GST-MUCI10 proteins were not active on glucomannan disaccharides and trisaccharides (Supplemental Fig. S8), these substrates may be too short to function as acceptors.

Our detailed characterization of the role of *MUCI10* in SCE cells significantly expands our knowledge of polysaccharide biosynthesis and demonstrates that wild-type Arabidopsis mucilage contains highly substituted GGM rather than unbranched glucomannan. This study highlights that, despite primarily consisting of pectin, Arabidopsis seed mucilage is a valuable model in which to study hemicellulose synthesis. We show that MUCI10 is responsible for GGM branching, which influences the distribution of pectin polymers and the structure of cellulose. Since GGM is the most abundant hemicellulose in the secondary walls of gymnosperms, understanding the biosynthesis of this polymer may facilitate improvements in the production of valuable commodities from softwoods. Further investigation of Arabidopsis natural variants with defects similar to *muci10* may allow us to identify additional genes involved in HM synthesis.

MATERIALS AND METHODS

Plant Material

Arabidopsis (*Arabidopsis thaliana*) mutants (*muci10-1*, SALK_061576; *muci10-2*, SALK_002556; *muci10-3*, SALK_133170; *muci10-4*, SALK_033930; *gt6-1*, SALK_134982; and *gt6-2*, SALK_151067) were selected from the SALK

collection (Alonso et al., 2003; http://signal.salk.edu/cgi-bin/tdnaexpress). The *cesa5-1* (SALK_118491; Mendu et al., 2011; Griffiths et al., 2014) and *csla2-3* (SALK_149092; Yu et al., 2014) mutants were described previously. The transfer DNA lines, Wave22Y (N781656) and ST-RFP (N799376) seeds, were ordered from the Nottingham Arabidopsis Stock Centre (http://arabidopsis.info). The Lm-2 (31AV), Ri-0 (160AV), and Lc-2 (171AV) accessions were obtained from the Versailles Arabidopsis Stock Center (http://publiclines.versailles.inra.fr). The plants were grown as described previously (Voiniciuc et al., 2015), in individual $7 \times 7 \times 8$-cm pots, under constant light (approximately 170 μE m^{-2} s^{-1}), temperature (20°C), and relative humidity (60%). Only the seeds analyzed in Supplemental Tables S2 and S3 were produced in a chamber with a 12/12-h photoperiod. Flowering plants were covered with ARACON tubes (Betatech; http://www.arasystem.com) to prevent the cross fertilization of flowers and seed dispersal. Seeds were harvested by shaking mature plants into individual brown paper bags.

Genotyping, RNA Isolation, and RT-PCR Analysis

The genotyping, RT-PCR, and cloning primers used are listed in Supplemental Table S4. PCR genotyping was performed using the Touch-and-Go method (Berendzen et al., 2005).

For RNA isolation, silique developmental stages were established along the stem length by dissecting seeds and analyzing the embryo stage. Counting the first open flower as 1, siliques 13+14 (heart stage), 20+21 (linear cotyledon), and 26+27 (mature green) were harvested for each genotype. Seed coat microarray data indicate that the heart stage and linear cotyledon stage are equivalent to 3 and 7 DPA, respectively (Dean et al., 2011; Belmonte et al., 2013). Whole siliques were immediately placed on dry ice and stored at –80°C. RNA was isolated using the ZR Plant RNA MiniPrep kit (Zymo Research; R2024) according to the manufacturer's instructions and included on-column DNase I (Zymo Research; E1009) digestion to remove any DNA contaminants. RNA was quantified using a NanoDrop 1000 (Thermo Fisher Scientific), and 200 ng was used as a template for the iScript cDNA Synthesis Kit (Bio-Rad; 170-8891). Primers for RT-PCR amplification were designed using the QuantPrime (http://www.quantprime.de) tool (Arvidsson et al., 2008). RT-PCR fragments were amplified for 33 cycles with Red-Taq DNA-Polymerase (VWR International; 733-2546P). *GLYCERALDEHYDE-3-PHOSPHATE DEHYDROGENASE C SUBUNIT1* was used as a reference gene (Dean et al., 2007), and DNA was stained with GelRed (Biotium). *UBIQUITIN5* served as a reference gene for qRT-PCR (Gutierrez et al., 2008). Amplification efficiencies were determined using a serial dilution of DNA, and the Pfaffl method was used to calculate fold changes in gene expression relative to the wild-type heart stage (Pfaffl, 2001; Fraga et al., 2008).

RR Staining

Staining was carried out using cell culture plates with 24 wells (VWR International; 734-2325). Around 30 seeds were added to a well prefilled with 500 μL of water and imbibed for 5 min with gentle mixing. After removing the water, seeds were stained with 300 μL of 0.01% (w/v) RR (VWR International; A3488.0001) for 5 min. The dye was replaced with 300 μL of water, and each well was imaged with a Leica MZ12 stereomicroscope equipped with a Leica DFC 295 camera. All images were analyzed and processed using Fiji (http://fiji.sc/Fiji; Schindelin et al., 2012).

Enzymatic digestion of mucilage capsules was also performed in a 24-well plate format. Dry seeds were imbibed in 500 μL of 0.1 M sodium acetate buffer, pH 4.5, with or without 10 units of the following enzymes (all from Megazyme): *Trichoderma longibrachiatum* endo-1,4-β-D-glucanase (E-CELTR), *Aspergillus niger* α-galactosidase (E-AGLAN), and/or *A. niger* endo-1,4-β-mannanase (E-BMANN). Plates were incubated for 50 to 90 min (as specified in the figures) at 125 rpm and 37°C to 40°C. The buffer was then removed, and each well was rinsed once with 500 μL of water prior to RR staining.

The effect of calcium cross links on mucilage dimensions was investigated by hydrating seeds in 500 μL of water, 50 mM $CaCl_2$, or 50 mM EDTA, pH 9.5, for 60 min at 125 rpm on a 24-well plate. Seeds were rinsed twice with water and then stained with RR.

Quantification of Mucilage Area

Image analysis followed ImageJ instructions (http://rsb.info.nih.gov/ij/docs/menus/analyze.html). Regions of interest were segmented in Fiji using distinct RGB Color Thresholding (minimum-maximum) parameters: mucilage + seed (Red 0-255, Green 0-115, and Blue 0-255) and seed (Red 0-120, Green 0-255, and Blue 0-255). Areas of the two regions of interest were measured using the Analyze Particles function (circularity = 0.5–1), excluding edges and extreme particle sizes, and were subtracted in Excel to calculate the dimensions of only the RR-stained mucilage capsules.

Statistical Analyses

The dimensions of mucilage capsules and their biochemical composition (see below) were normally distributed according to Shapiro and Wilk (1965), performed using the Real Statistics Resource Pack (http://www.real-statistics.com) for Microsoft Excel 2010. Statistically significant changes were identified through the T.TEST function in Microsoft Excel 2010, using two-tailed distribution and assuming equal variance of two samples.

The significant changes presented in Supplemental Figure S1 were identified using data obtained from the Bio-Analytic Resource (Winter et al., 2007; http://bar.utoronto.ca) and the unpaired Student's *t* test on the GraphPad Web site (http://www.graphpad.com/quickcalcs/ttest1/?Format=SD).

Total Mucilage Extraction and Monosaccharide Composition

Approximately 5 mg of seeds was precisely weighed in 2-mL Safe-Lock Eppendorf tubes. A serial dilution of a nine-sugar mixture (Fuc, Rha, Ara, Gal, Glc, Xyl, Man, GalUA, and GlcA; all obtained from Sigma-Aldrich) was performed in 2-mL screw-cap tubes. One milliliter of water, containing 30 μg of Rib as an internal standard, was added to all the samples and standards. Total mucilage was extracted by vigorously shaking the seed-containing tubes for 15 min at 30 Hz in a Retsch MM400 ball mill using two 24 TissueLyser Adapters (Qiagen). The adapters were then rotated 180° and mixed for an additional 15 min at 30 Hz. The seeds were allowed to settle at the bottom of each tube, and 800 μL of the supernatant was transferred to a screw-cap tube. Samples and standards were dried under pressurized air at 45°C using a Techne Dri-Block DB 3D heater. Once dry, 300 μL of 2 N trifluoroacetic acid (TFA) was added to each tube. Tubes were capped tightly, vortexed, and heated for 90 min at 121°C. The heating blocks and the samples were then cooled on ice. After brief centrifugation, tubes were uncapped and the TFA was evaporated under pressurized air at 45°C. Dried samples and standards were then resuspended in 400 μL of water. Monosaccharides were quantified by high-performance anion-exchange chromatography with pulsed amperometric detection (HPAEC-PAD) using a Dionex system equipped with a CarboPac PA20 column and GP50, ED50, and AS50 modules. The column was operated at a constant flow rate of 0.4 mL min^{-1} and was equilibrated with 2 mM NaOH for 10 min before sample injection. Neutral sugars were separated with 2 mM NaOH over the course of 18 min. Afterward, 513 mM NaOH was used for 7.5 min to separate uronic acids. Finally, the column was rinsed with 733 mM NaOH for 4 min. Monosaccharide amounts were normalized to the internal standard and quantified using standard calibration curves.

Quantification of Mucilage Detachment

Nonadherent and adherent mucilage fractions were sequentially extracted from 5 mg of seeds in 2-mL Safe-Lock Eppendorf tubes. Nonadherent mucilage was detached by mixing seeds in 1 mL of water for 15 min at 125 rpm using an orbital shaker, with 30 μg of Rib as an internal standard. Afterward, 800 μL of supernatants was transferred to 2-mL screw-cap tubes, dried, and prepared for HPAEC-PAD analysis similar to the total mucilage extracts.

After rinsing the seeds twice with water, the adherent mucilage was removed by essentially performing a total mucilage extraction, except that 2-deoxy-D-Glc was used as the internal standard instead of Rib. The supernatants were transferred to 2-mL screw-cap tubes, dried, and prepared for HPAEC-PAD analysis similar to the total mucilage extracts. Accordingly, the nine-sugar mixture dilutions were prepared using 2-deoxy-D-Glc as the internal standard.

Glycosyl Linkage Analysis of Total Mucilage Extracts

Total mucilage was extracted from 60 mg of seeds using the ball mill method described above. To obtain complete extraction, seeds were split into three 2-mL Safe-Lock Eppendorf tubes with 1 mL of water in each. Supernatants (800 μL) of the extractions were pooled, and 400 μL of the pooled sample was used for HPAEC-PAD monosaccharide analysis. The remaining sample was acidified by adding 800 μL of 0.1 M sodium acetate buffer, pH 4.6. The reduction of the uronic acids to their respective 6,6-dideuterio derivatives was carried out as described (Gibeaut and Carpita, 1991; Huang et al., 2011). For reduction, 0.1 mg

of 1-cyclohexyl-3-(2-morpholinyl-4-ethyl)carbodiimide (methyl-*p*-toluene sulfonate) was added to the samples. After 2 h of incubation, 0.1 mg of sodium borodeuteride together with 1 mL of cold 2 M imidazole, pH 7, was added, and the sample was incubated on ice for another 1 h. To remove residual sodium borodeuteride, glacial acid was added drop wise. After reduction of uronic acids, the samples were extensively dialyzed against water followed by lyophilization, and the dry samples were solubilized in 200 μL of anhydrous dimethyl sulfoxide (DMSO). Methylation was essentially performed as described (Gille et al., 2009). For the reaction, an alkaline DMSO solution was prepared using 100 μL of 50% (w/w) sodium hydroxide that was washed and sonicated several times with anhydrous DMSO (5 mL) and finally suspended in 2 mL of anhydrous DMSO. The alkaline DMSO suspension (200 μL), together with methyl iodide (100 μL), was added to samples. After 3 h of incubation, 2 mL of water was added to quench the reaction. Methylated polysaccharides were extracted with 2 mL of dichloromethane, hydrolyzed, derivatized to the corresponding alditol acetates, and analyzed by gas chromatography-mass spectrometry as described (Foster et al., 2010), using sodium borodeuteride for the reduction. Polysaccharide composition was calculated based on linkage analysis using a published protocol (Pettolino et al., 2012).

Monosaccharide Composition of Stem Alcohol-Insoluble Residue

The bottom 3 cm of the main inflorescence stem from 4-week-old Arabidopsis plants was harvested and immediately lyophilized. Dry stems were ground for 10 min at 30 Hz using a ball mill and steel balls. Afterward, 1 mL of 70% (v/v) aqueous ethanol was added, and the material was ground for an additional 10 min at 30 Hz. The insoluble residue was extracted once with 1:1 (v/v) chloroform:methanol and dried under a stream of air. HPAEC-PAD monosaccharide analysis of 2 mg of alcohol-insoluble residue (AIR) was performed similar to the total mucilage extracts, except that samples were shaken vigorously in 2 N TFA for 10 min at 20 Hz using a ball mill to fully disperse the AIR pellets prior to hydrolysis.

Crystalline Cellulose Observation and Content Determination

Seeds were hydrated in water for 10 min and examined on a glass slide with polarized light using a Zeiss Axioplan2 microscope equipped with a Zeiss AxioCam ICc 5 camera. For crystalline content determination, 5 mg of seeds was milled using steel balls for 90 s at 30 Hz. AIR was isolated by two sequential washes with 1 mL of 70% (v/v) ethanol and centrifugation for 3 min at 20,000*g*. After washing the AIR with 1:1 (v/v) chloroform:methanol, followed by acetone, the pellet was dried for 5 min at 60°C. Crystalline cellulose content was then determined as described previously (Foster et al., 2010), with minor modifications. The 2 mg of dry AIR was mixed with 1 mL of Updegraff reagent at 30 Hz for 90 s (Updegraff, 1969), before incubation at 100°C for 30 min. After hydrolysis, the Updegraff-resistant pellet (containing only crystalline cellulose) was rinsed once with water, once with acetone, dried, and then hydrolyzed using 200 μL of 72% (v/v) sulfuric acid. The amount of Glc released was quantified using anthrone on a 96-well plate (Foster et al., 2010).

LM22 ELISA Analysis of Nongalactosylated HM in Mucilage

The ELISA was performed as described (Pattathil et al., 2010), with minor modifications. We used bovine serum albumin instead of dry milk and a ready-to-use 3,3′,5,5′-tetramethylbenzidine substrate solution (Sigma-Aldrich; T4444-100ML). The 50-μL 3,3′,5,5′-tetramethylbenzidine reaction was stopped by adding 50 μL of 1 N sulfuric acid (instead of 0.5 N). All pipetting and wash steps were performed manually. Total mucilage was extracted from 10 mg of seeds using 1 mL of water, and 200-μL aliquots of the supernatant were transferred to a 96-well plate (Corning; 3598). Based on our monosaccharide data, these aliquots yield 0.4 μg of Man, which should be sufficient to saturate the wells with HM antigens. The LM22 antibody (PlantProbes; http://www.plantprobes.net) only effectively binds unbranched HM (Marcus et al., 2010).

Immunolabeling Experiments

Whole seeds were immunolabeled as described previously (Macquet et al., 2007) using LM21 (PlantProbes) and INRA-RU1 (Institut National de la Recherche Agronomique) primary antibodies (Marcus et al., 2010; Ralet et al., 2010). Alexa Fluor 488 (Molecular Probes, Life Technologies) was used as a secondary antibody. Observations were carried out on a Leica SP5 confocal microscope with settings fixed for the detection of the same label in different samples. LM21 labeling was analyzed with a Leica HyD detector (488-nm excitation and 500- to 550-nm emission). Images were processed identically in Fiji.

For crystalline cellulose labeling, seeds were first shaken in water. Unless stated otherwise, all incubations were performed for 60 min at 200 rpm using an orbital shaker. Seeds were rinsed twice with water and mixed with 800 μL of phosphate-buffered saline (PBS) for 30 min. The buffer was removed, and mucilage was blocked with 100 μL of 5% (w/v) bovine serum albumin in PBS. Seeds were sequentially incubated with 50 μL of His-tagged CBM3a (PlantProbes), anti-His mouse antibody (Sigma-Aldrich; SAB4600048), and Alexa Fluor 488 goat anti-mouse antibody. The primary antibody was diluted 1:10, while the secondary antibodies were diluted 1:1,000 using 1% (w/v) bovine serum albumin in PBS solution. Five PBS washes were performed after each of the three incubations. Seeds were counterstained for 20 min with 2.5% (w/v) calcofluor (Sigma-Aldrich; F3543), rinsed four times with water, and stored overnight in PBS at 4°C. Images were acquired on a Leica SP8 confocal microscope using the following settings: calcofluor (405-nm excitation and 405- to 452-nm emission) and CBM3a signal (488-nm excitation and 491- to 570-nm emission).

For cryosectioning, dry seeds were mounted in a mold (Dutscher; 040664), which was then completely filled with embedding medium (MM France; NEG50: F/161426) and frozen in liquid nitrogen. Thick (16–20 μm) sections were cut using a CryoStart NX70 (Thermo Scientific) at −20°C and were transferred onto a PolyLysine slide (Menzel Glaser, Thermo Scientific). For immunolabeling, frozen sections were first treated with 4% (w/v) formaldehyde in PBS for 15 min and then washed three times with PBS (5 min per wash). After blocking with 1% (w/v) milk protein in PBS for 60 min, sections were labeled with LM21 diluted 1:10 with 1% (w/v) milk protein in PBS for 120 min. After three PBS washes, sections were labeled with a goat anti-rat Alexa Fluor 488 (Molecular Probes, Life Technologies) secondary antibody diluted 1:100 with 1% (w/v) milk protein in PBS. Sections were washed three times with PBS and stained with either 0.1 mg mL^{-1} propidium iodide or 0.5% (w/v) calcofluor. After a final set of washes, sections were examined with a Leica SP5 or a Zeiss LSM 710 confocal microscope: calcofluor (405-nm excitation and 415- to 470-nm emission) and Alexa Fluor 488 (488-nm excitation and 500- to 550-nm emission).

Other Histological Techniques

The surface morphology of dry seeds, mounted onto a Peltier cooling stage with adhesive discs (Deben), was observed with a Hirox SH-1500 tabletop scanning electron microscope.

Cellulose was stained with 0.01% (w/v) S4B (now sold as Direct Red 23 [Sigma-Aldrich; 212490-50G]) in 50 mM NaCl (Anderson et al., 2010; Mendu et al., 2011) and was imaged with a Leica SP5 confocal system (561-nm excitation and 570- to 660-nm emission). Supplemental Figure S4 images were acquired using a Leica SP8 confocal system (552-nm excitation and 600- to 650-nm emission).

For Figure 9, RR-stained seeds were rinsed with water and counterstained with 200 μL of 0.025% (w/v) S4B in 50 mM NaCl for 60 min at 125 rpm. After three water washes, seeds were imaged using a the Leica SP8 confocal system (552-nm excitation and 600- to 650-nm emission).

For FITC-dextran staining in Supplemental Figure S4, seeds were imbibed in 1 mL of water in 2-mL Eppendorf tubes and rotated for 60 min at room temperature. The water was then replaced with 1 mL of 0.1 M citric acid and 0.2 M disodium phosphate, pH 5, and mixed for an additional 60 min. Seeds were transferred onto an eight-well sticky slide (Ibidi; 80828) and mixed with 250 μL of 0.1 M citric acid and 0.2 M disodium phosphate containing 250 μg of FITC-dextran (TdB Consultancy) for 60 min in the dark. FITC (488-nm excitation and 502- to 542-nm emission) was detected with a Leica SP5 confocal system.

For Figure 10, seeds were hydrated in 300 μL of 100 mM sodium acetate, pH 4.5, for 10 min and then stained with 300 μL of 1 mg mL^{-1} FITC-dextran 70-kD molecules (Sigma-Aldrich; 46945) for 30 min at 125 rpm on a 24-well plate. Seeds were transferred to glass slides and imaged with a Leica SP8 confocal system (488-nm excitation and 502- to 542-nm emission).

Expression and Analysis of MUCI10-sYFP Subcellular Localization

The *35S:MUCI10-sYFP* construct was generated using the ligation-independent cloning (LIC) technique (De Rybel et al., 2011). For cloning,

DNA was amplified with Phusion High-Fidelity DNA Polymerase (New England Biolabs). LIC-compatible pPLV vectors were obtained from the Nottingham Arabidopsis Stock Centre. We first amplified the sYFP (720 bp) tag from the pPLV16 vector and inserted it into the *Bam*HI site on the 3′ side of the LIC site in the pPLV25 vector (containing the 35S promoter but no fluorescent tag). The new *35S:LIC-sYFP* vector, named pCV01, was verified by Sanger sequencing. We redesigned the reverse LIC adapter primer to allow in-frame fusions to sYFP.

Arabidopsis wild-type genomic DNA was isolated using a commercial kit (GeneON; PT050). A *MUCI10* fragment (1,832 bp) was amplified from the ATG codon until, but excluding, the stop codon. The adapter primers required five three-step amplification cycles with a low annealing temperature (55°C) followed by 30 cycles of two-step Phusion PCR with an annealing/extension temperature of 72°C. The *MUCI10* amplicon was gel purified, and the rest of the LIC procedure was performed as described (De Rybel et al., 2011). The final plasmid was verified by Sanger sequencing and transformed into *Agrobacterium tumefaciens* GV3101::pMP90::pSOUP cells. Arabidopsis plants were then transformed using a modified floral spray method (Weigel and Glazebrook, 2006) with an infiltration medium containing 5% (w/v) Suc and 0.02% (v/v) Silwet L-77. Basta-resistant T1 seedlings were selected on soil using a 10 mg L^{-1} glufosinate-ammonium (Sigma-Aldrich; 45520-100MG) spray. Fluorescence was examined in Arabidopsis seedlings using a Leica SP8 confocal microscope: sYFP (488-nm excitation and 505- to 550-nm emission), intrinsic plant fluorescence (488-nm excitation and 615- to 705-nm emission), and RFP (552-nm excitation and 590- to 635-nm emission). To avoid cross talk for colocalization analysis, sYFP and RFP signals were sequentially acquired for each line scan.

Cloning of GST Protein Fusions

The topology of MUCI10 and GT6 proteins was assessed using ARAMEMNON (Schwacke et al., 2003). Truncated *MUCI10* (1,188 bp) and *GT6* (1,176 bp) sequences (lacking the 5′ region encoding an N-terminal transmembrane domain) were amplified from complementary DNA and inserted between the *Not*I and *Sal*I sites in the pGEX-5x-3 vector (GE Healthcare). This generated N-terminal fusions to GST. Plasmids were propagated in NEB 5-alpha *Escherichia coli* (New England Biolabs) and, after sequence verification, were transformed in BL21(DE3) *E. coli* (New England Biolabs) cells for protein expression.

GST Fusion Protein Expression and Purification

Protein expression and purification were performed in accordance with the pGEX guide (GE Healthcare). A 3-mL preculture of 2× YTA medium, containing ampicillin, was inoculated with BL21(DE3) *E. coli* containing the desired plasmid and incubated overnight at 37°C. The next day, the preculture was added to 100 mL of 2× YTA medium, containing ampicillin, and was incubated for 3 h until the optical density at 600 nm equaled 0.6. Protein expression was induced using 1 mM isopropyl β-D-1-thiogalactopyranoside (Carl Roth; 2316.2) for 16 h at 20°C. Cell pellets, collected using 7,100*g* at 4°C, were suspended in 2,500 μL of cold PBS buffer and disrupted on ice for 60 to 90 s using a Vibracell 75186 sonicator (pulse method, 50% intensity). Samples were then mixed with 62.5 μL of bacterial protease inhibitor (Carl Roth; 3758.1) and 125 μL of 20% (v/v) Triton X-100 on ice for 60 min. The lysate was cleared by spinning at 7,100*g* for 10 min at 4°C. For affinity purification, 2 mL of 50% (v/v) glutathione agarose slurry (Thermo Fisher Scientific Pierce) was added to gravity-flow columns and rinsed with 10 mL of 50 mM Tris-HCl and 150 mM NaCl, pH 8, equilibration buffer. Lysate, mixed with an equal volume of equilibration buffer, was added to the column. After rinsing with 10 mL of equilibration buffer, GST-tagged proteins were eluted using 50 mM Tris-HCl, 150 mM NaCl, and 10 mM reduced glutathione, pH 8. Purified proteins were quantified using the Qubit Protein Assay (Life Technologies).

UDP-Glo Assay for Galactosyltransferase Activity

The activity of GST-tagged proteins was quantified using the UDP-Glo glycosyltransferase assay (Promega; custom assay CS1681A05) according to the manufacturer's instructions and the GT reaction conditions that were successful for the IRX10-L xylan xylosyltransferase (Urbanowicz et al., 2014). GT reactions (25 μL) containing 50 mM HEPES-NaOH buffer (pH 7) and 1.25 μg of purified protein were carried out using 800 μM ultrapure UDP-Gal (Promega; V7171) as donor and 1 mM of an acceptor substrate. The acceptor substrates (all from Megazyme International) were mannotriose (O-MTR), mannotetraose (O-MTE), mannopentaose, (O-MPE), mannohexaose (O-MHE), cellohexaose (O-CHE), glucomannan disaccharides (O-GMMBI), and glucomannan trisaccharides (O-GMMTR). Cellohexaose, which XXTs bind to (Vuttipongchaikij et al., 2012), was included as a negative control. The galactosyltransferase reactions were incubated for 60 min at 23°C on a 96-well, half-area, white plate (VWR International; 392-0056). For UDP detection, 25 μL of UDP-Glo detection reagent was added to each reaction and incubated for 60 min at 23°C. The luminescence of each well was then measured using a Synergy H1M Hybrid Reader (BioTek). A serial dilution of UDP standards (Promega) showed a linear response from 0.01 to 12 μM.

Nicotiana benthamiana Microsome Preparation and Galactosyltransferase Assay

For transient expression in *N. benthamiana*, we created a *35S:MUCI10-YFP* construct by introducing the pDONR *MUCI10* clone obtained from the Joint BioEnergy Institute GT collection (Lao et al., 2014) into the pEarleyGate101 vector (Earley et al., 2006) using the LR Clonase II reaction according to the Life Technologies protocol. Constructs were verified by sequencing.

A. tumefaciens GV3101::pMP90 cells carrying the YFP fusion construct or the p19 gene from *Tomato bushy stunt virus* were grown overnight, pelleted at 4,000*g* (10 min and 15°C), washed, and resuspended in 10 mM MES, 10 mM $MgCl_2$, and 100 μM acetosyringone infiltration buffer, yielding a final optical density at 600 nm of 0.15. Leaves of 3- to 4-week-old *N. benthamiana* plants grown in a day/night cycle (16/8 h of light/dark, 25°C/24°C, and 60% relative humidity) were coinfiltrated with the two *A. tumefaciens* mixtures using a 1-mL syringe. After another 2 d of plant growth, protein expression was verified by monitoring YFP fluorescence with an epifluorescence microscope. Three days after infiltration, five entire leaves were harvested and microsomes were extracted (Rennie et al., 2012). Galactosyltransferase activity was determined essentially as described previously (Liwanag et al., 2012) using 40 μg of microsomal protein, 10 nCi of UDP-[^{14}C]Gal, and 20 mM mannohexaose per 50-μL reaction.

Supplemental Data

The following supplemental materials are available.

Supplemental Figure S1. *MUCI10* and *GT6* seed coat expression profiles.

Supplemental Figure S2. Overview of Fiji analysis to quantify mucilage.

Supplemental Figure S3. LM21 labeling of heteromannan in mucilage.

Supplemental Figure S4. S4B labeling of cellulose is reduced in *muci10*, *csla2*, and *cesa5*.

Supplemental Figure S5. CBM3a labeling of *muci10* and *csla2* single and double mutants.

Supplemental Figure S6. β-Glc digestion of extruded seed mucilage.

Supplemental Figure S7. Large FITC-dextrans cannot permeate mucilage.

Supplemental Figure S8. GGM mutants have normal seed surface morphology.

Supplemental Figure S9. LM21 labeling of mature seed cryo-sections.

Supplemental Figure S10. *MUCI10* and *GT6* do not affect stem AIR composition.

Supplemental Figure S11. Galactosyltransferase assays.

Supplemental Table S1. Seed and RR-stained mucilage dimensions.

Supplemental Table S2. Total mucilage content of seeds grown in a 12-h-light/12-h-dark photoperiod.

Supplemental Table S3. Nonadherent mucilage from seeds grown in a 12-h-light/12-h-dark photoperiod.

Supplemental Table S4. Genotyping, RT-PCR, and cloning primers.

ACKNOWLEDGMENTS

We thank Krešimir Šola and Dr. George Haughn (University of British Columbia) for the *cesa5-1* seeds.

Received June 22, 2015; accepted July 23, 2015; published July 28, 2015.

LITERATURE CITED

Alonso JM, Stepanova AN, Leisse TJ, Kim CJ, Chen H, Shinn P, Stevenson DK, Zimmerman J, Barajas P, Cheuk R, et al (2003) Genome-wide insertional mutagenesis of Arabidopsis thaliana. Science **301:** 653–657

Anderson CT, Carroll A, Akhmetova L, Somerville C (2010) Real-time imaging of cellulose reorientation during cell wall expansion in Arabidopsis roots. Plant Physiol **152:** 787–796

Arvidsson S, Kwasniewski M, Riaño-Pachón DM, Mueller-Roeber B (2008) QuantPrime: a flexible tool for reliable high-throughput primer design for quantitative PCR. BMC Bioinformatics **9:** 465

Belmonte MF, Kirkbride RC, Stone SL, Pelletier JM, Bui AQ, Yeung EC, Hashimoto M, Fei J, Harada CM, Munoz MD, et al (2013) Comprehensive developmental profiles of gene activity in regions and subregions of the Arabidopsis seed. Proc Natl Acad Sci USA **110:** E435–E444

Benová-Kákosová A, Digonnet C, Goubet F, Ranocha P, Jauneau A, Pesquet E, Barbier O, Zhang Z, Capek P, Dupree P, et al (2006) Galactoglucomannans increase cell population density and alter the protoxylem/metaxylem tracheary element ratio in xylogenic cultures of *Zinnia*. Plant Physiol **142:** 696–709

Ben-Tov D, Abraham Y, Stav S, Thompson K, Loraine A, Elbaum R, De Souza A, Pauly M, Kieber JJ, Harpaz-Saad S (2015) COBRA-LIKE 2, a member of the glycosylphosphatidylinositol-anchored COBRA-LIKE family, plays a role in cellulose deposition in Arabidopsis seed coat mucilage secretory cells. Plant Physiol **167:** 711–724

Berendzen K, Searle I, Ravenscroft D, Koncz C, Batschauer A, Coupland G, Somssich IE, Ulker B (2005) A rapid and versatile combined DNA/RNA extraction protocol and its application to the analysis of a novel DNA marker set polymorphic between *Arabidopsis thaliana* ecotypes Col-0 and Landsberg *erecta*. Plant Methods **1:** 4

Bernal AJ, Yoo CM, Mutwil M, Jensen JKJ, Hou G, Blaukopf C, Sørensen I, Blancaflor EB, Scheller HV, Willats WGT (2008) Functional analysis of the cellulose synthase-like genes *CSLD1*, *CSLD2*, and *CSLD4* in tip-growing Arabidopsis cells. Plant Physiol **148:** 1238–1253

Blake AW, McCartney L, Flint JE, Bolam DN, Boraston AB, Gilbert HJ, Knox JP (2006) Understanding the biological rationale for the diversity of cellulose-directed carbohydrate-binding modules in prokaryotic enzymes. J Biol Chem **281:** 29321–29329

Brown C, Leijon F, Bulone V (2012) Radiometric and spectrophotometric in vitro assays of glycosyltransferases involved in plant cell wall carbohydrate biosynthesis. Nat Protoc **7:** 1634–1650

Burton RA, Fincher GB (2012) Current challenges in cell wall biology in the cereals and grasses. Front Plant Sci **3:** 130

Burton RA, Gidley MJ, Fincher GB (2010) Heterogeneity in the chemistry, structure and function of plant cell walls. Nat Chem Biol **6:** 724–732

Caffall KH, Pattathil S, Phillips SE, Hahn MG, Mohnen D (2009) *Arabidopsis thaliana* T-DNA mutants implicate GAUT genes in the biosynthesis of pectin and xylan in cell walls and seed testa. Mol Plant **2:** 1000–1014

Cao J, Schneeberger K, Ossowski S, Günther T, Bender S, Fitz J, Koenig D, Lanz C, Stegle O, Lippert C, et al (2011) Whole-genome sequencing of multiple *Arabidopsis thaliana* populations. Nat Genet **43:** 956–963

Carpita N, Tierney M, Campbell M (2001) Molecular biology of the plant cell wall: searching for the genes that define structure, architecture and dynamics. Plant Mol Biol **47:** 1–5

Cavalier DM, Lerouxel O, Neumetzler L, Yamauchi K, Reinecke A, Freshour G, Zabotina OA, Hahn MG, Burgert I, Pauly M, et al (2008) Disrupting two *Arabidopsis thaliana* xylosyltransferase genes results in plants deficient in xyloglucan, a major primary cell wall component. Plant Cell **20:** 1519–1537

Chou YH, Pogorelko G, Young ZT, Zabotina OA (2015) Protein-protein interactions among xyloglucan-synthesizing enzymes and formation of Golgi-localized multiprotein complexes. Plant Cell Physiol **56:** 255–267

Chou YH, Pogorelko G, Zabotina OA (2012) Xyloglucan xylosyltransferases XXT1, XXT2, and XXT5 and the glucan synthase CSLC4 form Golgi-localized multiprotein complexes. Plant Physiol **159:** 1355–1366

Cocuron JC, Lerouxel O, Drakakaki G, Alonso AP, Liepman AH, Keegstra K, Raikhel N, Wilkerson CG (2007) A gene from the cellulose synthase-like C family encodes a beta-1,4 glucan synthase. Proc Natl Acad Sci USA **104:** 8550–8555

Cosgrove DJ (2005) Growth of the plant cell wall. Nat Rev Mol Cell Biol **6:** 850–861

Dagel DJ, Liu YS, Zhong L, Luo Y, Himmel ME, Xu Q, Zeng Y, Ding SY, Smith S (2011) In situ imaging of single carbohydrate-binding modules on cellulose microfibrils. J Phys Chem B **115:** 635–641

Dea ICM, Morris ER, Rees DA, Welsh EJ, Barnes HA, Price J (1977) Associations of like and unlike polysaccharides: mechanism and specificity in galactomannans, interacting bacterial polysaccharides, and related systems. Carbohydr Res **57:** 249–272

Dean G, Cao Y, Xiang D, Provart NJ, Ramsay L, Ahad A, White R, Selvaraj G, Datla R, Haughn G (2011) Analysis of gene expression patterns during seed coat development in *Arabidopsis*. Mol Plant **4:** 1074–1091

Dean GH, Zheng H, Tewari J, Huang J, Young DS, Hwang YT, Western TL, Carpita NC, McCann MC, Mansfield SD, et al (2007) The *Arabidopsis* MUM2 gene encodes a β-galactosidase required for the production of seed coat mucilage with correct hydration properties. Plant Cell **19:** 4007–4021

De Rybel B, van den Berg W, Lokerse A, Liao CY, van Mourik H, Möller B, Peris CL, Weijers D (2011) A versatile set of ligation-independent cloning vectors for functional studies in plants. Plant Physiol **156:** 1292–1299

Dhugga KS, Barreiro R, Whitten B, Stecca K, Hazebroek J, Randhawa GS, Dolan M, Kinney AJ, Tomes D, Nichols S, et al (2004) Guar seed beta-mannan synthase is a member of the cellulose synthase super gene family. Science **303:** 363–366

Dunkley TPJ, Hester S, Shadforth IP, Runions J, Weimar T, Hanton SL, Griffin JL, Bessant C, Brandizzi F, Hawes C, et al (2006) Mapping the *Arabidopsis* organelle proteome. Proc Natl Acad Sci USA **103:** 6518–6523

Dunkley TPJ, Watson R, Griffin JL, Dupree P, Lilley KS (2004) Localization of organelle proteins by isotope tagging (LOPIT). Mol Cell Proteomics **3:** 1128–1134

Earley KW, Haag JR, Pontes O, Opper K, Juehne T, Song K, Pikaard CS (2006) Gateway-compatible vectors for plant functional genomics and proteomics. Plant J **45:** 616–629

Eda S, Akiyama Y, Katō K, Ishizu A, Nakano J (1985) A galactoglucomannan from cell walls of suspension-cultured tobacco (*Nicotiana tabacum*) cells. Carbohydr Res **137:** 173–181

Edwards M, Scott C, Gidley MJ, Reid JS (1992) Control of mannose/galactose ratio during galactomannan formation in developing legume seeds. Planta **187:** 67–74

Edwards ME, Dickson CA, Chengappa S, Sidebottom C, Gidley MJ, Reid JSG (1999) Molecular characterisation of a membrane-bound galactosyltransferase of plant cell wall matrix polysaccharide biosynthesis. Plant J **19:** 691–697

Eronen P, Österberg M, Heikkinen S, Tenkanen M, Laine J (2011) Interactions of structurally different hemicelluloses with nanofibrillar cellulose. Carbohydr Polym **86:** 1281–1290

Faik A, Price NJ, Raikhel NV, Keegstra K (2002) An *Arabidopsis* gene encoding an alpha-xylosyltransferase involved in xyloglucan biosynthesis. Proc Natl Acad Sci USA **99:** 7797–7802

Foster CE, Martin TM, Pauly M (2010) Comprehensive compositional analysis of plant cell walls (lignocellulosic biomass) part I: lignin. J Vis Exp **37:** e1745

Fraga D, Meulia T, Fenster S (2008) Real-time PCR. *In* Current Protocols: Essential Laboratory Techniques. John Wiley & Sons, New York, pp 1–33

Geldner N, Dénervaud-Tendon V, Hyman DL, Mayer U, Stierhof YD, Chory J (2009) Rapid, combinatorial analysis of membrane compartments in intact plants with a multicolor marker set. Plant J **59:** 169–178

Gibeaut DM, Carpita NC (1991) Tracing cell wall biogenesis in intact cells and plants: selective turnover and alteration of soluble and cell wall polysaccharides in grasses. Plant Physiol **97:** 551–561

Gille S, Cheng K, Skinner ME, Liepman AH, Wilkerson CG, Pauly M (2011) Deep sequencing of voodoo lily (*Amorphophallus konjac*): an approach to identify relevant genes involved in the synthesis of the hemicellulose glucomannan. Planta **234:** 515–526

Gille S, Hänsel U, Ziemann M, Pauly M (2009) Identification of plant cell wall mutants by means of a forward chemical genetic approach using hydrolases. Proc Natl Acad Sci USA **106:** 14699–14704

Goubet F, Barton CJ, Mortimer JC, Yu X, Zhang Z, Miles GP, Richens J, Liepman AH, Seffen K, Dupree P (2009) Cell wall glucomannan in Arabidopsis is synthesised by CSLA glycosyltransferases, and influences the progression of embryogenesis. Plant J **60:** 527–538

Griffiths JS, Šola K, Kushwaha R, Lam P, Tateno M, Young R, Voiniciuc C, Dean G, Mansfield SD, DeBolt S, et al (2015) Unidirectional movement of cellulose synthase complexes in Arabidopsis seed coat

epidermal cells deposit cellulose involved in mucilage extrusion, adherence, and ray formation. Plant Physiol **168:** 502–520

Griffiths JS, Tsai AYL, Xue H, Voiniciuc C, Sola K, Seifert GJ, Mansfield SD, Haughn GW (2014) SALT-OVERLY SENSITIVE5 mediates Arabidopsis seed coat mucilage adherence and organization through pectins. Plant Physiol **165:** 991–1004

Gutierrez L, Mauriat M, Guénin S, Pelloux J, Lefebvre JF, Louvet R, Rusterucci C, Moritz T, Guerineau F, Bellini C, et al (2008) The lack of a systematic validation of reference genes: a serious pitfall undervalued in reverse transcription-polymerase chain reaction (RT-PCR) analysis in plants. Plant Biotechnol J **6:** 609–618

Handford MG, Baldwin TC, Goubet F, Prime TA, Miles J, Yu X, Dupree P (2003) Localisation and characterisation of cell wall mannan polysaccharides in *Arabidopsis thaliana*. Planta **218:** 27–36

Harpaz-Saad S, McFarlane HE, Xu S, Divi UK, Forward B, Western TL, Kieber JJ (2011) Cellulose synthesis via the FEI2 RLK/SOS5 pathway and cellulose synthase 5 is required for the structure of seed coat mucilage in Arabidopsis. Plant J **68:** 941–953

Haughn GW, Western TL (2012) *Arabidopsis* seed coat mucilage is a specialized cell wall that can be used as a model for genetic analysis of plant cell wall structure and function. Front Plant Sci **3:** 64

Huang J, DeBowles D, Esfandiari E, Dean G, Carpita NC, Haughn GW (2011) The Arabidopsis transcription factor LUH/MUM1 is required for extrusion of seed coat mucilage. Plant Physiol **156:** 491–502

Keegstra K (2010) Plant cell walls. Plant Physiol **154:** 483–486

Keegstra K, Cavalier D (2010) Glycosyltransferases of the GT34 and GT37 families. Annu Plant Rev **41:** 235–249

Kong Y, Zhou G, Abdeen AA, Schafhauser J, Richardson B, Atmodjo MA, Jung J, Wicker L, Mohnen D, Western T, et al (2013) GALACTURONOSYLTRANSFERASE-LIKE5 is involved in the production of Arabidopsis seed coat mucilage. Plant Physiol **163:** 1203–1217

Kremers GJ, Goedhart J, van Munster EB, Gadella TWJ Jr (2006) Cyan and yellow super fluorescent proteins with improved brightness, protein folding, and FRET Förster radius. Biochemistry **45:** 6570–6580

Lao J, Oikawa A, Bromley JR, McInerney P, Suttangkakul A, Smith-Moritz AM, Plahar H, Chiu TY, González Fernández-Niño SM, Ebert B, et al (2014) The plant glycosyltransferase clone collection for functional genomics. Plant J **79:** 517–529

Liepman AH, Nairn CJ, Willats WGT, Sørensen I, Roberts AW, Keegstra K (2007) Functional genomic analysis supports conservation of function among cellulose synthase-like A gene family members and suggests diverse roles of mannans in plants. Plant Physiol **143:** 1881–1893

Liepman AH, Wilkerson CG, Keegstra K (2005) Expression of cellulose synthase-like (Csl) genes in insect cells reveals that CslA family members encode mannan synthases. Proc Natl Acad Sci USA **102:** 2221–2226

Liwanag AJM, Ebert B, Verhertbruggen Y, Rennie EA, Rautengarten C, Oikawa A, Andersen MCF, Clausen MH, Scheller HV (2012) Pectin biosynthesis: GALS1 in *Arabidopsis thaliana* is a β-1,4-galactan β-1,4-galactosyltransferase. Plant Cell **24:** 5024–5036

Lombard V, Golaconda Ramulu H, Drula E, Coutinho PM, Henrissat B (2014) The Carbohydrate-Active Enzymes Database (CAZy) in 2013. Nucleic Acids Res **42:** D490–D495

Macquet A, Ralet MC, Kronenberger J, Marion-Poll A, North HM (2007) In situ, chemical and macromolecular study of the composition of *Arabidopsis thaliana* seed coat mucilage. Plant Cell Physiol **48:** 984–999

Manzanares P, de Graaff LH, Visser J (1998) Characterization of galactosidases from *Aspergillus niger*: purification of a novel alpha-galactosidase activity. Enzyme Microb Technol **22:** 383–390

Marcus SE, Blake AW, Benians TAS, Lee KJD, Poyser C, Donaldson L, Leroux O, Rogowski A, Petersen HL, Boraston A, et al (2010) Restricted access of proteins to mannan polysaccharides in intact plant cell walls. Plant J **64:** 191–203

Mendu V, Griffiths JS, Persson S, Stork J, Downie AB, Voiniciuc C, Haughn GW, DeBolt S (2011) Subfunctionalization of cellulose synthases in seed coat epidermal cells mediates secondary radial wall synthesis and mucilage attachment. Plant Physiol **157:** 441–453

Millane RP, Hendrixson TL (1994) Crystal structures of mannan and glucomannans. Carbohydr Polym **25:** 245–251

Mutwil M, Obro J, Willats WGT, Persson S (2008) GeneCAT: novel webtools that combine BLAST and co-expression analyses. Nucleic Acids Res **36:** W320–W326

Nebenführ A, Ritzenthaler C, Robinson DG (2002) Brefeldin A: deciphering an enigmatic inhibitor of secretion. Plant Physiol **130:** 1102–1108

Nikolovski N, Rubtsov D, Segura MP, Miles GP, Stevens TJ, Dunkley TPJ, Munro S, Lilley KS, Dupree P (2012) Putative glycosyltransferases and other plant Golgi apparatus proteins are revealed by LOPIT proteomics. Plant Physiol **160:** 1037–1051

Nikolovski N, Shliaha PV, Gatto L, Dupree P, Lilley KS (2014) Label-free protein quantification for plant Golgi protein localization and abundance. Plant Physiol **166:** 1033–1043

North HM, Berger A, Saez-Aguayo S, Ralet MC (2014) Understanding polysaccharide production and properties using seed coat mutants: future perspectives for the exploitation of natural variants. Ann Bot (Lond) **114:** 1251–1263

Obayashi T, Okamura Y, Ito S, Tadaka S, Aoki Y, Shirota M, Kinoshita K (2014) ATTED-II in 2014: evaluation of gene coexpression in agriculturally important plants. Plant Cell Physiol **55:** e6

Pattathil S, Avci U, Baldwin D, Swennes AG, McGill JA, Popper Z, Bootten T, Albert A, Davis RH, Chennareddy C, et al (2010) A comprehensive toolkit of plant cell wall glycan-directed monoclonal antibodies. Plant Physiol **153:** 514–525

Pauly M, Gille S, Liu L, Mansoori N, de Souza A, Schultink A, Xiong G (2013) Hemicellulose biosynthesis. Planta **238:** 627–642

Pauly M, Keegstra K (2010) Plant cell wall polymers as precursors for biofuels. Curr Opin Plant Biol **13:** 305–312

Pettolino FA, Walsh C, Fincher GB, Bacic A (2012) Determining the polysaccharide composition of plant cell walls. Nat Protoc **7:** 1590–1607

Pfaffl MW (2001) A new mathematical model for relative quantification in real-time RT-PCR. Nucleic Acids Res **29:** e45

Preston RD (1968) Plants without cellulose. Sci Am **218 (6):** 102–108

Ralet MC, Tranquet O, Poulain D, Moïse A, Guillon F (2010) Monoclonal antibodies to rhamnogalacturonan I backbone. Planta **231:** 1373–1383

Rautengarten C, Usadel B, Neumetzler L, Hartmann J, Büssis D, Altmann T (2008) A subtilisin-like serine protease essential for mucilage release from Arabidopsis seed coats. Plant J **54:** 466–480

Rennie EA, Hansen SF, Baidoo EE, Hadi MZ, Keasling JD, Scheller HV (2012) Three members of the Arabidopsis glycosyltransferase family 8 are xylan glucuronosyltransferases. Plant Physiol **159:** 1408–1417

Rodríguez-Gacio MdelC, Iglesias-Fernández R, Carbonero P, Matilla ÁJ (2012) Softening-up mannan-rich cell walls. J Exp Bot **63:** 3976–3988

Saez-Aguayo S, Ralet MC, Berger A, Botran L, Ropartz D, Marion-Poll A, North HM (2013) PECTIN METHYLESTERASE INHIBITOR6 promotes *Arabidopsis* mucilage release by limiting methylesterification of homogalacturonan in seed coat epidermal cells. Plant Cell **25:** 308–323

Scheller HV, Ulvskov P (2010) Hemicelluloses. Annu Rev Plant Biol **61:** 263–289

Schindelin J, Arganda-Carreras I, Frise E, Kaynig V, Longair M, Pietzsch T, Preibisch S, Rueden C, Saalfeld S, Schmid B, et al (2012) Fiji: an open-source platform for biological-image analysis. Nat Methods **9:** 676–682

Schwacke R, Schneider A, van der Graaff E, Fischer K, Catoni E, Desimone M, Frommer WB, Flügge UI, Kunze R (2003) ARAMEMNON, a novel database for Arabidopsis integral membrane proteins. Plant Physiol **131:** 16–26

Shapiro SS, Wilk MB (1965) An analysis of variance test for normality (complete samples). Biometrika **52:** 591–611

Sims IM, Craik DJ, Bacic A (1997) Structural characterisation of galactoglucomannan secreted by suspension-cultured cells of *Nicotiana plumbaginifolia*. Carbohydr Res **303:** 79–92

Srivastava M, Kapoor VP (2005) Seed galactomannans: an overview. Chem Biodivers **2:** 295–317

Sullivan S, Ralet MC, Berger A, Diatloff E, Bischoff V, Gonneau M, Marion-Poll A, North HM (2011) CESA5 is required for the synthesis of cellulose with a role in structuring the adherent mucilage of Arabidopsis seeds. Plant Physiol **156:** 1725–1739

Suzuki S, Li L, Sun YH, Chiang VL (2006) The cellulose synthase gene superfamily and biochemical functions of xylem-specific cellulose synthase-like genes in *Populus trichocarpa*. Plant Physiol **142:** 1233–1245

Teh OK, Moore I (2007) An ARF-GEF acting at the Golgi and in selective endocytosis in polarized plant cells. Nature **448:** 493–496

Updegraff DM (1969) Semimicro determination of cellulose in biological materials. Anal Biochem **32:** 420–424

Urbanowicz BR, Peña MJ, Moniz HA, Moremen KW, York WS (2014) Two Arabidopsis proteins synthesize acetylated xylan in vitro. Plant J **80:** 197–206

Vasilevski A, Giorgi FM, Bertinetti L, Usadel B (2012) LASSO modeling of the *Arabidopsis thaliana* seed/seedling transcriptome: a model case for detection of novel mucilage and pectin metabolism genes. Mol Biosyst **8:** 2566–2574

Voiniciuc C, Dean GH, Griffiths JS, Kirchsteiger K, Hwang YT, Gillett A, Dow G, Western TL, Estelle M, Haughn GW (2013) Flying saucer1 is a transmembrane RING E3 ubiquitin ligase that regulates the degree of pectin methylesterification in *Arabidopsis* seed mucilage. Plant Cell **25:** 944–959

Voiniciuc C, Yang B, Schmidt MH, Günl M, Usadel B (2015) Starting to gel: how Arabidopsis seed coat epidermal cells produce specialized secondary cell walls. Int J Mol Sci **16:** 3452–3473

Vuttipongchaikij S, Brocklehurst D, Steele-King C, Ashford DA, Gomez LD, McQueen-Mason SJ (2012) *Arabidopsis* GT34 family contains five xyloglucan α-1,6-xylosyltransferases. New Phytol **195:** 585–595

Wang Y, Alonso AP, Wilkerson CG, Keegstra K (2012) Deep EST profiling of developing fenugreek endosperm to investigate galactomannan biosynthesis and its regulation. Plant Mol Biol **79:** 243–258

Wang Y, Mortimer JC, Davis J, Dupree P, Keegstra K (2013) Identification of an additional protein involved in mannan biosynthesis. Plant J **73:** 105–117

Warde-Farley D, Donaldson SL, Comes O, Zuberi K, Badrawi R, Chao P, Franz M, Grouios C, Kazi F, Lopes CT, et al (2010) The GeneMANIA prediction server: biological network integration for gene prioritization and predicting gene function. Nucleic Acids Res **38:** W214–W220

Weigel D, Glazebrook J (2006) In planta transformation of *Arabidopsis*. Cold Spring Harb Protoc 2006: pdb.prot4668

Willats WGT, McCartney L, Knox JP (2001) In-situ analysis of pectic polysaccharides in seed mucilage and at the root surface of *Arabidopsis thaliana*. Planta **213:** 37–44

Winter D, Vinegar B, Nahal H, Ammar R, Wilson GV, Provart NJ (2007) An "Electronic Fluorescent Pictograph" browser for exploring and analyzing large-scale biological data sets. PLoS ONE **2:** e718

Yin L, Verhertbruggen Y, Oikawa A, Manisseri C, Knierim B, Prak L, Jensen JK, Knox JP, Auer M, Willats WGT, et al (2011) The cooperative activities of CSLD2, CSLD3, and CSLD5 are required for normal *Arabidopsis* development. Mol Plant **4:** 1024–1037

Yu L, Shi D, Li J, Kong Y, Yu Y, Chai G, Hu R, Wang J, Hahn MG, Zhou G (2014) CELLULOSE SYNTHASE-LIKE A2, a glucomannan synthase, is involved in maintaining adherent mucilage structure in Arabidopsis seed. Plant Physiol **164:** 1842–1856